Pergamon

Int. J. Multiphase Flow Vol. 22, No. 5, pp. 923–952, 1996
Published by Elsevier Science Ltd
Printed in Great Britain
PII: S0301-9322(96)00041-9 0301-9322/96 $15.00 + 0.00

THE ROLE OF GAS PERMEATION IN CONVECTIVE BURNING

B. W. ASAY, S. F. SON and J. B. BDZIL
Los Alamos National Laboratory, Los Alamos, NM 87545, U.S.A.

(Received 20 November 1995; in revised form 29 May 1996)

Abstract—Convective burning is commonly identified in the literature as the key step in deflagration-to-detonation transition (DDT) of granular explosives. The prevalent physical picture of convective burning is of rapid and *deep* penetration of hot gases which controls the propagation rate via convective heat transfer. This investigation includes a review of relevant literature, new transient measurements of permeability at high pressures, and analysis of the experimental results. Results presented here show that *deep* penetration (many particle diameters) of gas at high velocities is not physically plausible for the low porosity granular beds of interest. The measured permeabilities are consistent with measurements made at lower pressures in similar materials, but are significantly lower than predictions based on beds of spherical particles. The important time and space scales of this experiment are identified. The interface region between the reservoir and porous bed is analysed. The wave hierarchy of the permeation experiment is studied, and short- and long-time limits are investigated using simplified asymptotic analysis. The low-speed flow approximation is also considered for flow within the bed. It is shown that drag dissipation terms in the energy equation cannot be neglected under adiabatic conditions as is commonly done. These results indicate that compaction processes play a larger role than commonly thought, and motivate the consideration of an asymptotic large drag limit of two-phase, two-velocity models. Published by Elsevier Science Ltd.

Key Words: gas permeation in porous beds, convective burning, explosives, energetic materials, combustion, deflagration-to-detonation transition (DDT)

1. INTRODUCTION

Deflagration-to-detonation transition (DDT) has been responsible for both accidental and intentional detonations since explosive materials were first used. After more than 50 years of scientific research, quantitative *prediction* of DDT is still not generally possible. In some cases, observed phenomena cannot even be qualitatively linked to known physical processes. Unless these processes are understood, it will be difficult to design and implement better safety measures.

Because of the numerous dependent processes and scales present in this problem, the mechanisms and parameters exerting the greatest influence need to be clearly identified and more thoroughly studied. Only then can there be hope of developing a tractable, predictive model. To determine the relative importance of different mechanisms, it is essential to quantify the temporal and spatial scales of the various processes. In this paper we address the step in a DDT event that is almost universally cited as being the most crucial element; that is, convective burning.

First, the relevant literature is reviewed. Then, results from permeation experiments in low-porosity granular beds are presented and analysed. These results quantify the temporal and spatial scales of the permeation expected to occur during convective burning in low-porosity granular beds. The results indicate that the convective burning flame structure must be significantly different than commonly envisioned, and that compaction mechanisms play a large role in DDT. The relevance of these results to convective burning modeling is then discussed.

2. BACKGROUND

2.1. Separate stages of DDT

The literature on the subject of DDT is voluminous and a complete review will not be attempted. Several published reviews exist (Bernecker & Price 1974a; Bernecker & Price 1974b; Bernecker & Price 1974c; Belyaev *et al.* 1975; Gockhale & Krier 1982; Bernecker 1986) and the reader is referred

to them for a more extensive treatment. Here we present a brief overview of the *generally accepted* stages which lead to DDT.

The energy transfer mechanism by which the hot combustion products heat the fresh material to the ignition point strongly influences the speed of the resulting combustion wave. The progress of a reaction wave from deflagration-to-detonation has been postulated to occur in four stages (cf. Belyaev *et al.* 1975). The first is characterized as layer-by-layer, or normal burning. Propellant in a solid rocket motor generally burns in this mode and propagation rates are on the order of 1 cm/s. The heat transfer from the gas phase (combustion products) to the solid (fresh material) is predominantly conductive. The pressures obtained with this mode of burning are not sufficient to drive the shock formation required to achieve detonation. The second stage, widely considered to be the crucial trigger for DDT, consists of convective burning, with propagation rates on the order of 100 m/s. It has been speculated that rapid permeation of hot combustion gases far ahead of the flame front is the dominant energy transport mechanism during this stage. Third, a regime termed compressive burning begins in which reaction is predominantly initiated by compaction waves. This has sometimes been called "low velocity detonation" (LVD). Ultimately, a steady state detonation initiated by shock waves is achieved.

As a preface to this work, we will briefly review three topics: (a) convective burning, (b) permeation of gases through porous beds, and (c) multiphase continuum modeling. An extensive literature base exists for each of these areas. Here we will only discuss the major elements which have direct bearing on this work.

2.2. *Convective burning*

Because convective combustion is seen by many as the most important step in the sequence leading to DDT, it merits careful study. Figure 1 illustrates schematically the transition from normal burning to convective burning observed in large volume high pressure vessels called Crawford bombs (cf. Fifer & Cole 1981). These bombs are used to isolate and study normal and convective burning. At lower pressures the regression rate is slow (normal burning) and is comparable to that found in full density materials. Above a critical pressure, however, a sharp increase in the burning rate with a further increase in pressure is observed. This transition from normal burning to convective burning occurs at lower pressures in beds with larger pore sizes. Russian workers (cf. Ermolaev *et al.* 1975) argue that the transition is related to the standoff distance (gas phase preheat and reaction zone). They argue that if the standoff distance is larger

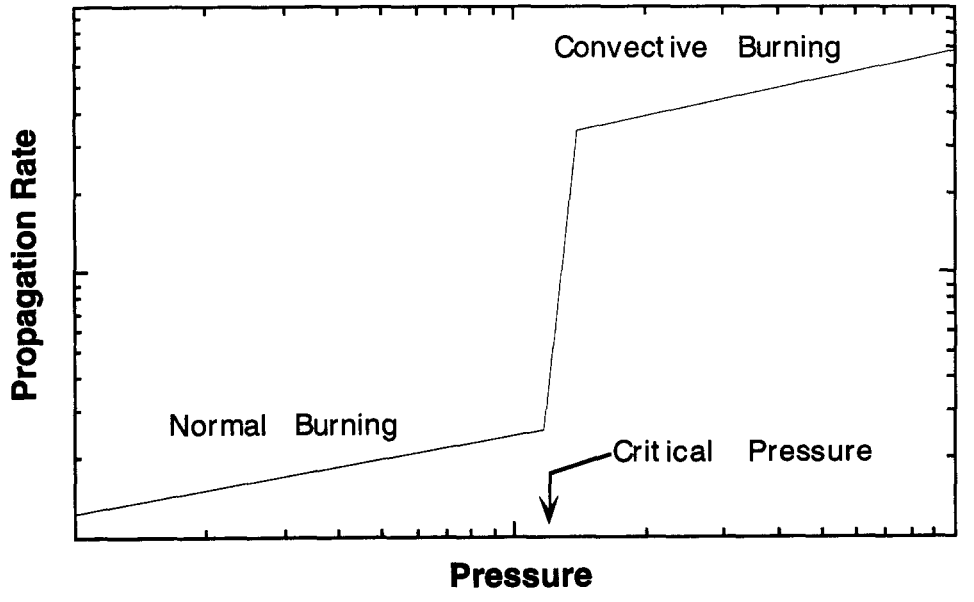

Figure 1. Schematic of the burning rate as a function of pressure for a granular bed burning in a Crawford (large volume) bomb.

Table 1. Classical definitions of convective burning

"[Convective burning is] hot combustion products being forced ahead of the reaction zone into the unchanged explosive" (Griffiths & Groocock 1960).
"[Convective burning is] the penetration of gases deep inside a burning powdered explosive, caused by the dynamic increase in pressure" (Andreev & Chuiko 1963).
"[Heat transfer in the convective burning regime is by] forced convection" (Belyaev *et al.* 1975).
"Combustion products...penetrate through the pores† into the unreacted explosive, overtake the flame front and preheat the walls of the pores up to the ignition point" (Sulimov *et al.* 1976).

†"Pores" refers to intergranular, rather than intragranular, passages.

than the pore size, the flame cannot spread into the bed. Based on this idea they have successfully correlated the critical pressure to standoff distance relative to the pore diameter.

A complete discussion of even this stage of DDT is difficult because of the wide range of possible experimental conditions that directly affect the outcome. Bulk densities can potentially range from nearly zero (dusty gases) to theoretical maximum density (TMD). This work is limited to low porosity (low gas volume fraction) granular beds (≤ 0.3) that represent damaged explosives. Next we define what is typically meant by the term convective burning, as well as discuss evidence that has been used to support this concept.

Definition. It is difficult to find a precise definition in the literature for "convective burning". However, because this mechanism has been widely described as the trigger mechanism of DDT, it is imperative that the definition be unambiguous. Representative statements made by researchers in this area are summarized in table 1. Most of the primary references are found in the Russian literature. These have formed the foundation of much of the DDT research (particularly the modeling). Thus, for brevity, only the primary sources are shown here.

These concepts clearly define convective burning as a deflagration wave whose propagation rate is controlled by convective heat transfer via rapid, *deep* penetration of hot gases, instead of

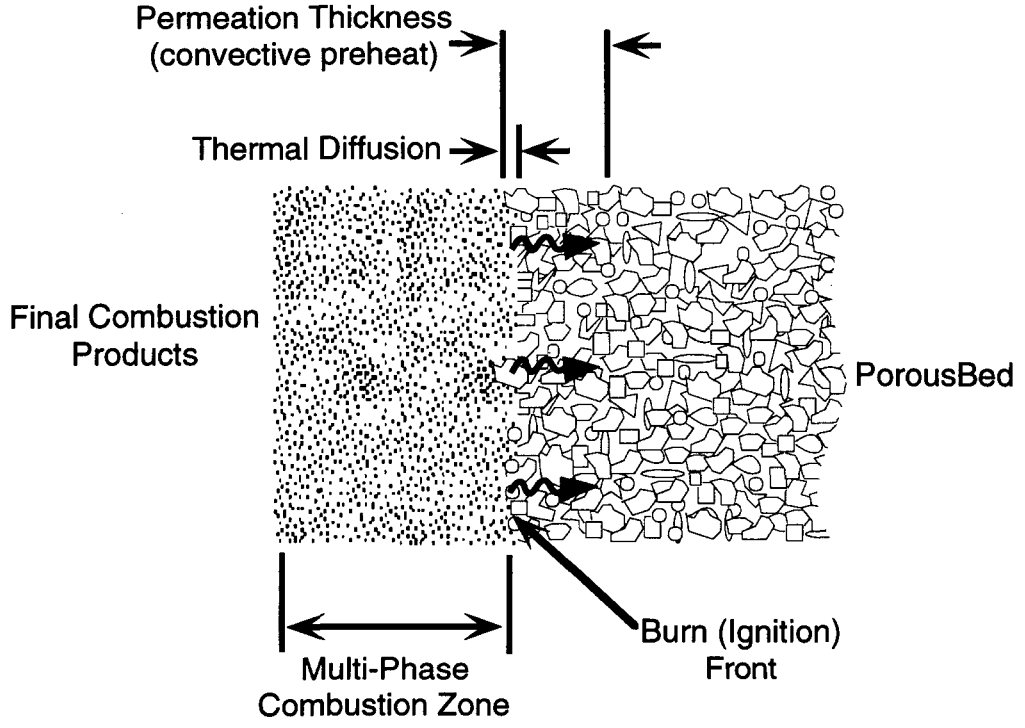

Figure 2. Schematic of convective burning. A thick permeation layer (many particle lengths) ahead of the ignition front is shown; however, this work shows that such a thick permeation layer is not plausible. A diffusive zone preceding the ignition front is also shown. Such a zone has been neglected in previous work since diffusive mechanisms are too slow to yield the fast propagation rates observed. The ignition front is followed by a multiphase combustion zone.

Table 2. Importance of rapid burning in the transition to detonation†

"The *penetration* of combustion into the the pores *due to convective heat transfer* is the *basic cause* of the acceleration of combustion in porous explosive systems. There is *no doubt* that ignition of the explosive by a convective gas flow is the basic form of excitation of the chemical reaction in the initial stage of predetonation development of the process" (Korotkov *et al.* 1969).
"...penetration of the gaseous products into the pores and the development of convective regimes are the *intial and principal reason* for the acceleration of combustion" (Obmenin *et al.* 1969).
"The model is based on the experimental evidence that convective burning is *led* by hot gases penetrating through larger pores" (Sulimov *et al.* 1976).
"The increase in mass burning velocity with decreasing density indicates the presence of convective heat transfer from the burning zone to the unreacted substance and limited penetration of the combustion products into the existing pores. It has now been convincingly proved that the impairment of stability during deflagration arises due to the filtration of gaseous products into the pores" (Belyaev *et al.* 1975).
"Convective combustion is the *major stage* in the combustion-to-detonation transition in porous fuels... Directly ahead of the convective front, the difference between gas and particle velocities in the initial stage is relatively great" (Akhatov & Vainshtein 1983).

†Key words have been italicized for emphasis.

diffusional processes only. A schematic of this process is shown in figure 2. The permeation layer is shown as the leading part of the wave structure. In figure 2 we have shown a thick permeation layer (many particle lengths) as generally assumed. This may not be the case, as we will show in this work. The permeation could be followed by a diffusive zone preceding the ignition front. Generally such a zone has been neglected in previous work since diffusive mechanisms are thought to be too slow to yield the fast propagation rates observed. However, Drew (1986) included a diffusive zone in his analysis of convective burning. The ignition front is followed by a multiphase combustion zone where particles are eventually consumed (Fifer & Cole 1981). The physical picture of rapid and deep penetration of gases deep into unburned material is also firmly entrenched in more recent literature. For example, Drew (1986) assumed a thick convective preheat zone in approximate analytical solutions of the steady convective burning wave. Also, Baer & Nunziato (1986) interpreted simulation results with this conceptual picture in mind.

The postulated mechanism driving this deep and rapid gas penetration is a pressure gradient, either static or dynamic (Belyaev *et al.* 1975). In the static pressure mechanism, the pressure at the surface of the hot charge exceeds the pressure in the granular bed (Belyaev *et al.* 1975), resulting in a bulk movement of gas through the intergranular pores. The dynamic pressure mechanism involves the formation of individual gas jets. Jets are formed because the pore openings between the particles are curved. Gases issuing from these curved surfaces collide and form high velocity streams of combustion products, producing local pressure elevations which force the jets into the intragranular pores. These pressure gradients are *claimed* to yield rapid, deep penetration of hot gases into the unburned bed.

When the statements and figures are taken together, a clear picture of the conventional definition of convective combustion emerges. It consists of hot gases penetrating far ahead (up to several tube diameters) of the combustion front. These gases preheat the particles to ignition.

Importance. The importance of the convective burning mechanism has been emphasized many times. Representative statements are presented in table 2.

Evidence. Here we review the experimental evidence that has been interpreted by some to support the classical concept of convective burning and the conclusion that it is an important step in DDT. The classical mechanism of convective combustion appears credible because there are a vast number of experimental observations that have been examined based on this physical picture, and the model often appears to, at least qualitatively, adequately explain most observed behavior. However, nearly all of the evidence cited is indirect, owing to limitations of instrumentation in the harsh multiphase combustion environment and the complexity of the problem. This indirect evidence is then interpreted within the classical paradigm of convective burning. The experimental evidence falls into four primary areas: effects on burning velocity, critical pressure, transition distance, and combustion environment, and is summarized in tables 3–6.

Many of the methods for diagnosing the initiation and progression of this assumed mechanism are unreliable. For example the reliability of optical records of the ignition front (often the primary

Table 3. Burn velocity effects

As pressure increases, a critical pressure is reached which causes the combustion rate to increase dramatically (rapid burning occurs). It is argued that once this critical pressure is reached, the gases are forced deep into the bed of particles and at that point convective heat transfer becomes the dominant mode of heat transfer which controls the rapid burning (Andreev & Chuiko 1963; Bobolev *et al.* 1966).
As the charge diameter increases, the propagation rate increases. It is argued that this occurs because as one increases the diameter, the relative proportion of large pores compared to small pores increases, thus increasing the ability of the gas to permeate deeply into the bed (Belyaev *et al.* 1975).
As the relative density increases, the burning rate increases to a maximum, and then decreases (Belyaev *et al.* 1975). Andreev & Chuiko (1963) note that this trend may not be attributable directly to the burning characteristics of "convective" burning, but that the dependence is most likely the result of a decrease in dilution by the inert pressurizing gas as the relative density increases.

support provided for this mechanism) can be questionable. Optical records of the front are incapable of giving a complete and objective picture of the occurrence and development of convective combustion (Belyaev *et al.* 1966; Belyaev *et al.* 1975). Reasons for this include the fact that individual grains can obstruct the viewing window (Pozhariskii & Ivanov 1993), breakdown of stable burning occurs first at the largest pores, not uniformly (Belyaev *et al.* 1966), and the spread of the flame is chaotic (Dubovitskii *et al.* 1974). Furthermore, it is often difficult to distinguish between compressive (including compaction effects) and convective effects in experiments and modeling (Bdzil & Son 1995). Difficulties of similar magnitude are encountered with other experimental techniques designed to shed light on the mechanism of convective combustion. For example, results from experiments in Crawford bombs are complicated because the gas (usually nitrogen) used to pressurize the bomb, infiltrates the pores before the experiment (see table 6).

In some cases, the published literature in this area does not adequately characterize the experimental conditions considered. For example, Dubovitskii *et al.* (1974) state that the results of their experiments and modeling show that the filtration zone (zone of penetrating gases) is 15–20 mm, the heating zone (diffusive zone) is 4 mm and the chemical reaction zone is 1–2 mm thick. They also reported that as the combustion temperature increases, the width of these zones decreases. However, important parameters such as the initial porosity of the system were not reported. This is an important omission because, based upon photographic evidence, it has generally been concluded that the size of the nonuniformity in the flame front (interpreted as the permeation thickness) is fairly large and can reach several charge diameters (Belyaev *et al.* 1975).

Table 4. Critical pressure effects

It has been found that as the explosive particle size increases, the critical pressure decreases (Belyaev *et al.* 1966; Bobolev *et al.* 1966). This effect is attributed to the change in packing and pore size distribution.
As the porosity is increased the critical pressure decreases (Belyaev *et al.* 1966). Similar data show that as the permeability is increased, the critical pressure decreases (Andreev & Chuiko 1963; Belyaev *et al.* 1966). These two parameters exert a similar, albeit somewhat independent, effect.
The charge diameter also has an effect on the critical pressure (Belyaev *et al.* 1966). The critical pressure decreases as diameter increases up to approximately 10 mm, but the effect is negligible at larger diameters. This agrees with the effect on burning velocity.
Critical pressure is also affected by the charge length. It was found that if the end of the tube opposite the ignitor is sealed, under certain conditions the critical pressure is not reached (Belyaev *et al.* 1966). They propose that gases permeating into the charge pressurize the explosive ahead of the flame front, decreasing the pressure gradient, and stabilizing the combustion. Thus, convective combustion is inhibited.
The combustion temperature of the explosive exerts a large effect on the achievement of convective burning. It has been found (Belyaev *et al.* 1975) that as the combustion temperature is increased through compositional changes, the critical pressure decreases. The gas products resulting from explosives having higher combustion temperature are supposedly more effective at preheating the explosive ahead of the flame front.
One author (Taylor 1962a; Taylor 1962b) suggested that a continuous melt layer on the surface of an explosive particle would stabilize the flame by preventing intrusion of hot gases into the pores between particles. He calculated melt layer thicknesses and correlated these with stability measurements using critical pressure as the figure of merit. He found that indeed, the relationship was qualitatively correct. Others (Belyaev *et al.* 1966; Belyaev *et al.* 1975) extended the work and obtained results consistent with the proposal that the melt layer functions as a gas tight membrane, preventing diffusion of gaseous products into the pores. Explosives that do not melt were typically found to have much lower critical pressures than explosives that do melt.

Table 5. Transition distance effects

The position at which a deflagration becomes a detonation, relative to the ignition point, is known as the transition distance. This distance is a function of porosity and permeability. Both of these effects are used as evidence for the convective combustion mechanism.

It has been reported (Korotkov *et al.* 1969) that as the porosity increases from a low value, the transition distance decreases and then increases. The porosity at which the minimum occurs is a function of the particle size. This effect is explained in terms of the rate of pressure increase. The porosity at which the minimum in critical pressure occurs is postulated as providing the conditions for the maximization in pressurization rate. At higher porosities, the excess volume is too great, while at lower porosities, the specific pore surface area affected by combustion is too small to afford the most rapid increase in pressure with time. A similar effect has been noted using permeability as the independent variable (Griffiths & Groocock 1960).

However, Sulimov *et al.* (1976) found that monosize pore distributions have substantially thicker permeation zones than do bimodal distributions. They reason that this occurs because larger pores facilitate the penetration of gases. Pore size distribution is only one of a multitude of variables that can influence experimental observations.

2.3. Permeation of gases through porous beds

Characterizing the permeation of gases in porous beds is an important step in determining the plausibility of mechanisms thought to occur in convective burning. Permeability (κ) is generally used to characterize permeation. It is the proportionality constant in Darcy's law and is a measure of the ease with which a fluid permeates into a porous solid. Most measurements of permeability are performed quasistaticially; that is, a constant pressure source is applied to a bed of known porosity. The flow rate is measured and the permeability is calculated. Often these measurements are made in materials that differ significantly from granular explosives. Recently Shepherd & Begeal (1988) made dynamic and quasistatic measurements on explosives, inert simulants, and glass beads using ambient temperature nitrogen as the driving fluid. Pressures from 0.69 to 138 MPa were used. Isothermal conditions were assumed in their analysis. The authors concluded that, for quasistatic conditions, empirical correlations calibrated to beds of spherical particles predicted the measured permeabilities beds of glass beads adequately. At porosities of approximately 20%, the range of measured permeabilities were $10^{-12} \leqslant \kappa \leqslant 10^{-10}\,\mathrm{cm}^2$. However, for the explosive CP composed of nonspherical particles, empirical correlations for spherical particles over-predicted permeabilities by factors of 5–50. They also compared numerical solutions to transient experimental results using models based on the work of Morrison (1972; 1976; 1977) and Nilson (1981). The pulse shape and transit times through beds of glass beads compared favorably with predictions. The permeabilities obtained from the transient experiments were similar to those obtained from quasistatic testing. However, higher Reynolds numbers can be obtained using transient methods. In the permeation experiments of explosives and inerts described above, a drag coefficient δ of about $2.0 \times 10^8\,\mathrm{kg/m^3\,s}$ for granular explosive materials with porosities, ϕ_G, near 0.3 was obtained. The drag coefficient is inversely related to the permeability (see [1]) and is formally defined later with the governing equations (see [3]). The pressures considered by Shepherd and Begeal are below those which can occur in convective burning. The permeation rate is a result of the interplay between the driving potential (pressure gradient) and resistive force (drag). Consequently an objective in our work was to quantify the resistance to flow under conditions of higher driving pressures in low porosity granular beds.

2.4. Modeling of convective burning

Several models have been proposed to describe convective burning in granular energetic materials. The goal of early work was to model flame propagation in packed beds of granular

Table 6. Effect of combustion environment

The Crawford bomb is a constant-pressure device. The manometric bomb has a much smaller volume than does the Crawford bomb, and thus the pressure increases as combustion proceeds. The critical pressures that are determined from each of these devices are much different. The critical pressures determined for a given explosive using the manometric bomb are 10–15 times lower than those found using the Crawford bomb to "the filling of the pores with cold inert gas in the pressurizing process, which leads to a substantial reduction in the pressure drop causing diffusion of the combustion products into the pores and to the intense cooling of these products".

propellants under confinement, with an emphasis on gun cartridge applications (Kuo *et al.* 1973; Kuo & Summerfield 1974; Krier *et al.* 1976; Kuo *et al.* 1976). Later models were proposed that extended this earlier work to describe the transition from convective burning to detonation. A review of such models is found in Gockhale & Krier (1982). More recently, Drew (1986) used asymptotic methods to obtain predictions of the propagation rate of a convective combustion wave. Drew assumed a low Mach number flow, a thick permeation zone, and efficient heat transfer between the particles and the gas. Drag relations based on empirical expressions fit to permeation experiments in beds of spherical particles were used in these models. Stewart *et al.* (1994) provide a good review of the origins of the two phase modeling approach and address the problem using a simplified scheme.

The DDT model of Baer & Nunziato (1986) used the drag correlations obtained by Shepherd & Begeal (1988) for low-porosity granular beds. A "permeation" zone 15 mm thick was identified by Baer and Nunziato on pressure profiles 20 μs into a calculation (see figure 13 in Baer & Nunziato (1986)). In order for gases to penetrate into the unreacted bed this distance in this amount of time, the velocity difference between the gas and solid must be on average 750 m/s. However, examination of published results from similar simulations shows that the gas and particle velocities are nearly equal (less than 10 m/s differences) everywhere (see figure 6 in Baer & Nunziato (1986)). Clearly, this structure cannot be attributable to permeation. Similar structures have been obtained by considering only compaction effects (no drag interaction) in numerical simulations (Bdzil & Son 1995). The structure calculated by Baer and Nunziato most likely arises from compaction and reaction processes, and not deep, rapid penetration of gases into the bed. Others (Ermolaev *et al.* 1975) also claim to predict thick "permeation" zones (again with a porosity of 30%, the reported filtration zone is 10 cm, the heating zone is 1.4 mm, and the combustion zone is 5 mm). Interpreting results in these complex multi-process problems must be done with great care.

2.5. Drag coefficient

The key parameter in modeling permeation is the drag coefficient (or, inversely, the permeability). The Forchheimer equation (Forchheimer 1901) is often used to model the drag coefficient,

$$\delta = \frac{\mu_G}{\kappa} + \frac{\lambda \rho_G \phi_G}{\kappa} |u_G|, \qquad [1]$$

where κ, μ_G, and λ are the permeability, gas viscosity, and Forchheimer constant. The gas phase density and velocity are denoted by ρ_G and u_G, respectively. The drag law, [1], can be further simplified by assuming that either the viscous (first term) or the inertial (second term) term dominates. When the viscous terms dominate, the Forchheimer relationship reduces to Darcy's law. Typically, κ and λ are correlated to such parameters as effective particle diameter and porosity. MacDonald *et al.* (1979) give various expressions for these relationships. The following section describes the permeation experiments that were designed to characterize the permeation rate in low porosity granular beds driven by high pressure gradients.

3. EXPERIMENTAL DETERMINATION OF PERMEABILITY AT HIGH PRESSURE

To characterize permeation under conditions similar to those experienced in convective burning (in particular, high driving pressures and low porosities) an apparatus was designed that used burning explosive to rapidly pressurize a reservoir adjoining an inert low-porosity packed bed. Pressures up to 621 MPa with pressurization times in the reservoir of less than 1 ms were attained. A schematic of the apparatus used to measure permeability is shown in figure 3. The burn chamber was a steel tube into which a Pyrofuse hot wire ignitor was placed. A mixture of titanium and boron (Ti-B) was placed inside a Teflon ring and in contact with the Pyrofuse. Class A HMX high-explosive powder was then poured on top of the Ti-B and lightly tamped. The total volume of the burn chamber was 1200 mm^3. The amount of HMX was varied to obtain different maximum pressures. Silicon carbide (SiC) was used as the porous bed. SiC was chosen because of its high melting temperature and strength. The SiC was packed into a steel tube of slightly smaller diameter

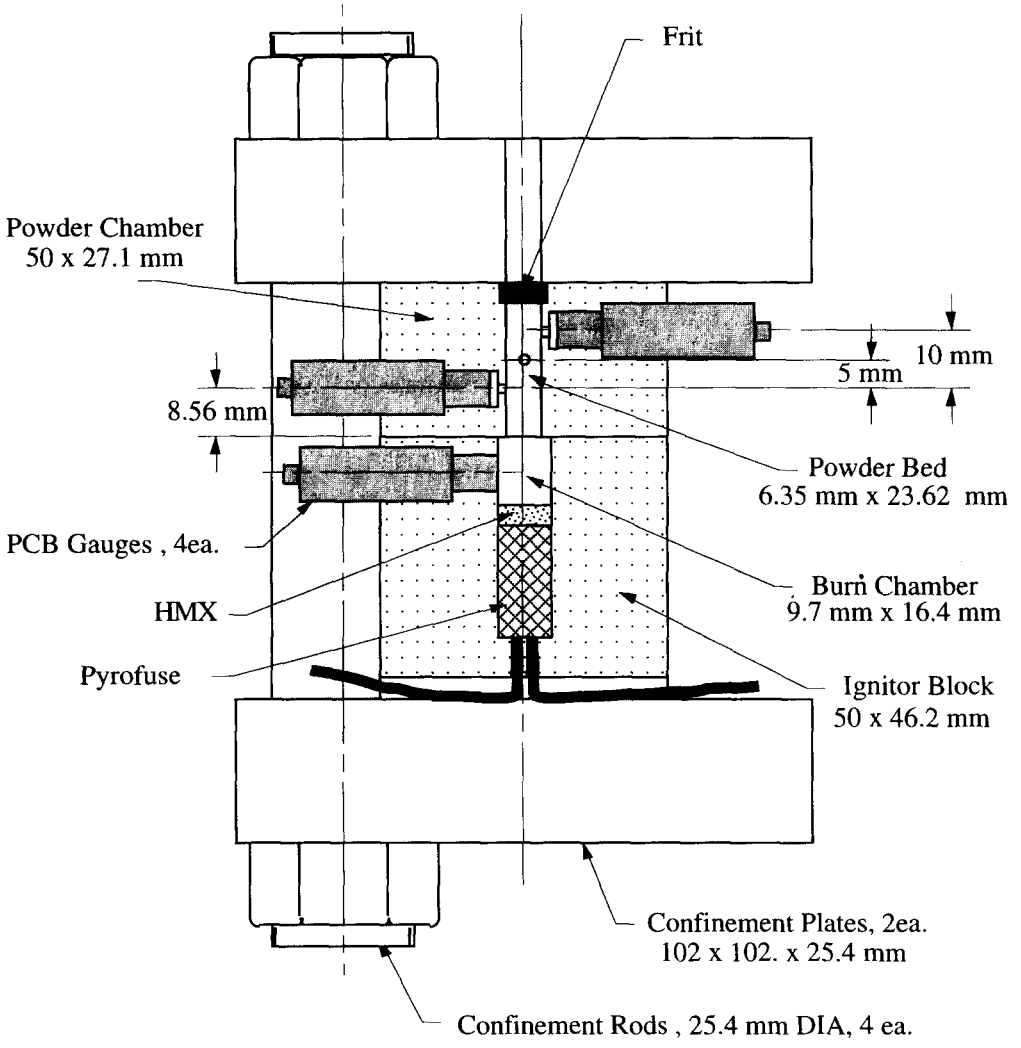

Figure 3. Schematic of permeation experiments. A Pyrofuse hot wire ignitor was used to ignite low density HMX in the burn chamber. The amount of HMX was varied to obtain different maximum pressures. Silicon carbide (SiC) was used as the porous bed. SiC was chosen because of its high melting temperature and strength.

using a ram press and a pressure of approximately 27 MPa. Final SiC densities were approximately 74% of the theoretical maximum density (TMD, 3.217 g/cm^3). Porosities in damaged explosives are expected to be generally lower. Thus, this is considered a worst case. The particle size distribution is shown in figure 4. The SiC particles used were nonspherical (see figure 5), which is typical of granular explosives. The entire assembly was then clamped between two steel plates using four threaded rods. A stainless steel frit (Cajon, model EL) was placed at the chamber exit.

Four piezoelectric transducers (PCB, Model 109-A02) were used to measure dynamic pressures. One gauge was placed in the burn chamber and three others were distributed along the wall of the powder chamber as shown in figure 3. The locations of the gauges relative to the interface (positive into the bed) were -11.8, 8.56, 13.56 and 18.56 mm for gauges 1–4, respectively.

After each test, the SiC bed was visually examined. Total compression of the bed was less than a millimeter, and the particles at the burn chamber/particle bed interface were usually fused slightly to a depth of 1–2 mm, indicating some surface softening had occurred. This observation indicates that rapid heating occurred for a short time near the interface, and is consistent with simulations presented later. The SiC bed beyond the interface region appeared unchanged except for minor darkening of the original color, which diminished with distance from the interface.

The testing procedure consisted of first applying a voltage (12 V) to the Pyrofuse. Several

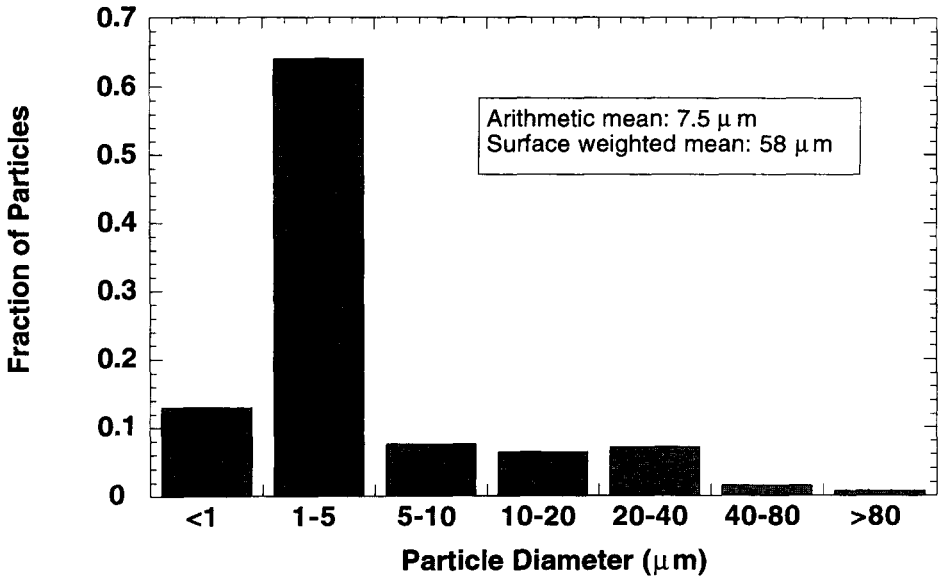

Figure 4. SiC particle size distribution measured using microscopic Bioscan Imaging Analysis.

milliseconds passed before the hot Ti-B particles ignited the HMX grains. Once the pressure in the burn chamber began to rise, the digitizers were triggered to record the pressure transducer output. A respresentative record of one experiment is shown in figure 6. Three peak reservoir pressure levels were considered: 162, 310, and 621 MPa. The modeling and analysis is described in the following section. The experimental results are presented in a later section.

Figure 5. Photograph of representative SiC particles used.

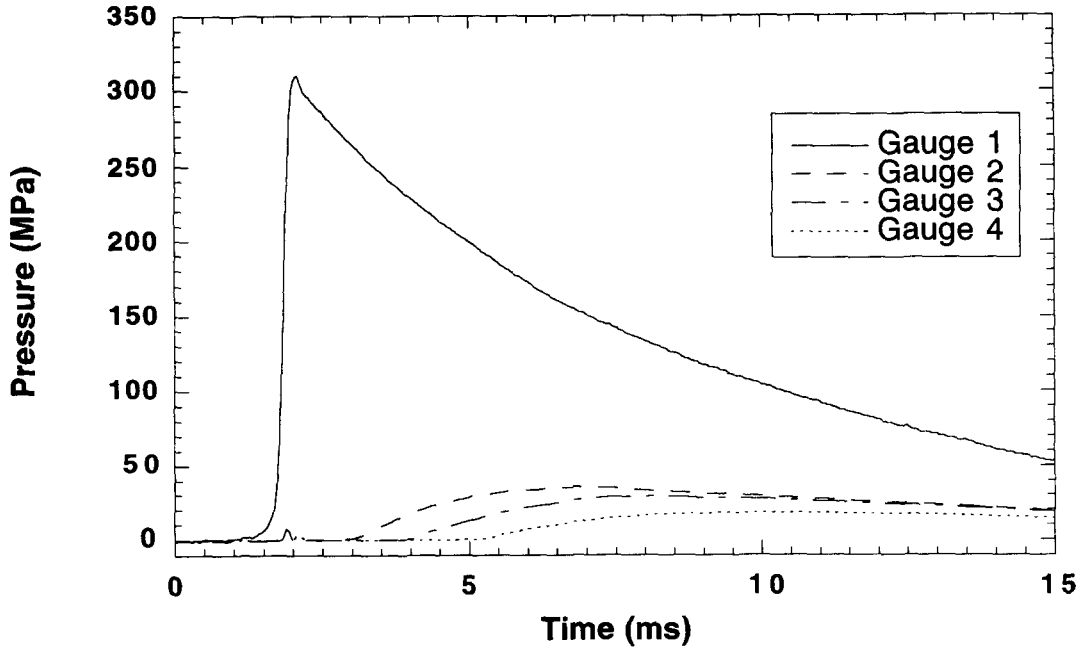

Figure 6. Results from a typical permeation experiment.

4. MODELING

A simplified version of the BN model (Baer & Nunziato 1986; Bdzil & Son 1995) was adopted. The solid is assumed to be incompressible and stationary (no compaction). Within these assumptions, the equations for mass conservation are

Gas mass
$$\frac{\partial}{\partial t}(\phi_G \rho_G) + \frac{\partial}{\partial x}(\phi_G \rho_G u_G) = 0, \quad [2a]$$

and

Solid mass
$$\frac{\partial}{\partial t}(\phi_S \rho_S) = 0. \quad [2b]$$

Here ϕ is the volume fraction, ρ is the density, and u is the velocity. The subscripts, S and G, refer to the solid and gas phases, respectively. Conservation of momentum is described by,

Gas momentum
$$\frac{\partial}{\partial t}(\phi_G \rho_G u_G) + \frac{\partial}{\partial x}(\phi_G \rho_G u_G^2 + \phi_G p_G) = -p_G \frac{\partial \phi_S}{\partial x} - \delta u_G, \quad [3a]$$

for the gas phase and,

Solid momentum
$$\frac{\partial}{\partial x}(\phi_S p_S) = p_G \frac{\partial \phi_S}{\partial x} + \delta u_G, \quad [3b]$$

for the solid phase. The pressure is denoted by p, and δ is the drag coefficient. The equations for conservation of energy are,

Gas energy
$$\frac{\partial}{\partial t}(\phi_G \rho_G (e_G + u_G^2/2)) + \frac{\partial}{\partial x}[u_G(\phi_G \rho_G (e_G + u_G^2/2) + \phi_G p_G)] = H(T_S - T_G), \quad [4a]$$

and

Solid energy
$$\frac{\partial}{\partial t}(\phi_S \rho_S e_S) = -H(T_S - T_G), \quad [4b]$$

where e, H, and T represent the specific internal energy, the heat transfer coefficient, and the temperature. The saturation condition is $\phi_G + \phi_S = 1$. Heat conduction within each phase has been

neglected. Given the assumptions of an incompressible solid, and that the bed is not allowed to move (i.e. a force is applied to the far end of the bed), [2b] and [3b] do not need to be considered.

We model the burn chamber by assuming that the pressurization due to the burning HMX is instantaneous. The combustion gas is considered to obey an ideal gas law (a good approximation for these experiments)

$$p_G = (\gamma - 1)C_{vG}\rho_G T_G, \qquad [5]$$

where γ is the adiabatic constant (ratio of specific heats) and C_{vG} is the specific heat at constant volume for the gas. For this problem $\gamma = 1.23$ and $C_{vG} = 1.9 \times 10^3$ J/kg K. A representative initial state of the burned HMX is $\rho_{G0} = 168$ kg/m^3, $P_{G0} = 2.94 \times 10^8$ Pa, and $T_{G0} = 4000$ K. The dimensions of the burn chamber are such that it is large compared to the acoustic scale of interest and small compared to the long-time permeation scale. That is, we consider the burn chamber to be infinite on the acoustic scale and essentially a uniform state on the permeation scale. Therefore, we associate no spatial scales with the burn chamber.

4.1. Scalings and reduced equations

The equations for modeling the gas flow through the SiC bed contain three separate spatial scales: (1) a drag scale related to δ, (2) a heat transfer scale related to H, and (3) the thickness associated with $(\partial\phi_S/\partial x)^{-1}$ at the interface region between the gas reservoir and the SiC bed. The heat transfer coefficient is a function of the gas flow and is estimated to be in the range 3.7×10^7 W/m^3 K $\leqslant H \leqslant 4.4 \times 10^{10}$ W/m^3 K. Similarly for the drag coefficient the range is estimated to be 2.0×10^8 kg/m^3 s $\leqslant \delta \leqslant 2.2 \times 10^{11}$ kg/m^3 s. To get these estimates we have assumed gas speeds ranging from zero to 1500 m/s and $\phi_S = 0.74$. The density and "energy" scalings are taken to be $\rho_{G0}\phi_{G0} = 45$ kg/m^3 and $\gamma(\gamma - 1)C_{vG} = 540$ J/kg K, respectively. Using these parameters the permeation and heat transfer time scales (the subscripts p and h correpond to permeation and heat transfer, respectively) are

$$2 \times 10^{-10}\text{ s} \leqslant t_p \equiv \frac{\phi_{G0}\rho_{G0}}{\delta} \leqslant 2 \times 10^{-7}\text{ s}, \qquad [6]$$

and

$$5.5 \times 10^{-7}\text{ s} \leqslant t_h \equiv \frac{(\phi_{G0}\rho_{G0})\gamma(\gamma - 1)C_{vG}}{H} \leqslant 7 \times 10^{-4}\text{ s}. \qquad [7]$$

Therefore, we expect as the gas permeates through the bed it decelerates orders of magnitude faster than the time required for heat transfer from the hot combustion gases to the bulk of the SiC. Initially we will neglect heat transfer to the bed since it is a much slower process than the drag. We choose to use the drag scaling as our principal scale. Because the shortest distances in the bed are related to the acoustic processes, we use the initial sound speed of the representative burn chamber gases, $c_{G0} = 1.5 \times 10^3$ m/s, to form a spatial scale

$$x_p \equiv \frac{c_{G0}\phi_{G0}\rho_{G0}}{\delta} = 3 \times 10^{-4}\text{ m}, \qquad [8]$$

where we have assumed that $\delta = 2.0 \times 10^8$ kg/m^3 (this value corresponds to the estimated value for the low-speed value of δ for this bed).

The last scale we consider represents some measure of the thickness of the interface region between the burn chamber and the bed as measured by $\phi_{S0}(\partial\phi_S(x)/\partial x)^{-1}$. Although we have no direct measure of this, it is probably related to the SiC particle size

$$x_n \equiv \phi_{S0}\left(\frac{\partial\phi_S(x)}{\partial x}\right)^{-1} = 6 \times 10^{-5}\text{ m}, \qquad [9]$$

where the subscript n refers to the interface region.

On neglecting heat transfer, the entire dynamics of the permeation problem is describable with only the gas phase equations. Using the ideal gas law for the specific internal energy (see [5]) and

t_p and x_p as the time and space scales, [2a], [3a] and [4a] can be rewritten in Lagrangian (particle based) form as

$$\frac{DR}{D\tau} + R\frac{\partial U}{\partial \xi} = -\frac{RU}{\epsilon_n}\left(\frac{1}{\phi_G}\right)\frac{d\phi_G}{d\zeta}, \quad [10]$$

$$R\frac{DU}{D\tau} + \frac{1}{\gamma}\frac{\partial P}{\partial \xi} = -\left(\frac{U}{\phi_G}\right), \quad [11]$$

and

$$\frac{1}{\gamma}\frac{DP}{D\tau} - \frac{P}{R}\frac{DR}{D\tau} = \frac{(\gamma-1)U^2}{\phi_G}, \quad [12]$$

where

$$\tau \equiv t/t_p, \quad \xi \equiv x/x_p, \quad \frac{D}{D\tau} \equiv \frac{\partial}{\partial \tau} + U\frac{\partial}{\partial \xi}, \quad [13]$$

$$\zeta \equiv x/x_n, \quad \epsilon_n \equiv x_n/x_p \ll 1, \quad [14]$$

and

$$P \equiv p_G/p_{G0}, \quad R \equiv \rho_G/\rho_{G0}, \quad U \equiv u_G/c_{G0}, \quad [15]$$

with $c_{G0}^2 \equiv \gamma p_{G0}/\rho_{G0}$. The source terms in [10]–[12] represent two physical processes with differing spatial scales; the $O(1)$ drag scale and the $O(\epsilon_n) = O(10^{-1})$ nozzling scale. The drag process contributes to the production of entropy in [12] while the interface region nozzling term, $(1/\phi_G)(d\phi_G/d\zeta)$, does not.

Because the scale of these processes is different, we consider sequential limits with each process treated separately. Although the nozzling term at the interface region is not the principal concern of this paper, we treat it here because it controls the flow of gas into the SiC bed. In the next subsection we consider the action of the nozzling on the "interface" condition.

4.2. Interface region

The gas permeation problem we consider is fundamentally a two-phase, two-velocity flow. In such flows, the phase pressure and particle velocity can be discontinuous at "interfaces." The connection conditions for the states on either side of the interface region are controlled by a structure problem driven by the nozzling term. Here we consider this structure problem for an interface region that, due to the incompressible nature of the SiC bed, remains stationary.

The interface region represents the shortest scale considered in this problem. Because the dynamics on either side of the interface occur on slower time scales, we can consider the flow in the non-dissipative, interface region to be quasi-steady; that is, no explicit time dependence is considered. Scaling the distance coordinate with respect to the nozzling scale, $\xi = \epsilon_n\zeta$ and assuming that all the dependent variables are $O(1)$, yields the interface region equations (analogous to the standard nozzle equations)

$$\frac{d}{d\zeta}(RU) = -RU\left(\frac{1}{\phi_G}\right)\frac{d\phi_G}{d\zeta}, \quad [16]$$

$$RU\frac{dU}{d\zeta} + \frac{1}{\gamma}\frac{dP}{d\zeta} = 0, \quad [17]$$

and

$$\frac{1}{\gamma}\frac{dP}{d\zeta} - \frac{P}{R}\frac{dR}{d\zeta} = 0. \quad [18]$$

Equation [18] gives the isentropic relation $P/R^{\gamma} = 1$ and integrating [16] across the interface region, yields,

$$\frac{U_r}{U_b} = \phi_{Gb}\left(\frac{P_b}{P_r}\right)^{1/\gamma}, \qquad [19]$$

where the subscripts r and b denote the burn chamber (reservoir) and bed, respectively. Rewriting [16]–[18] and using $c^2 = P^{(\gamma-1)/\gamma}$, yields the nozzling equation (cf. Thompson (1972), p. 281)

$$\frac{dM^2}{d\zeta} = M^2\left\{\frac{(\gamma-1)M^2+2}{M^2-1}\right\}\left(\frac{1}{\phi_G}\right)\frac{d\phi_G}{d\zeta}, \qquad [20]$$

where $M^2 \equiv U^2/c^2$ is the square of the Mach number. The important observation here, is that if $M_r^2 < 1$ and ϕ_G decreases monotonically in going from the reservoir to the bed, with $(d\phi_G/d\zeta)$ limiting to zero in the bed, then $M_b^2 \leqslant 1$. This is analogous to a converging nozzle in single phase flow. From [19] and [20] it follows that for the conditions of our problem, the flow accelerates going through the interface region limited only by $M_b^2 = 1$, which corresponds to choked flow. The nozzling action of the interface in conjunction with the high pressure reservoir gas serves to generate a high-speed flow near the interface in this problem.

Integrating [20] gives us the "interface" jump condition

$$M_b^2 = \frac{2}{(\gamma-1)}\left\{\frac{(\psi^{\gamma-1}-1)}{\psi^{\gamma-1}(\phi_{Gb}^2\psi^2-1)}\right\}, \qquad [21]$$

subject to the condition that $M_b^2 \leqslant 1$ and where $\psi \equiv (P_b/P_r)^{1/\gamma}$. Equations [19] and [21] connect the flows at either side of the interface region. Importantly, when the pressure jump across the interface region goes to zero, the flow of gas into the bed stops. In the next subsection, we consider the flow that develops in this problem in response to a jump in pressure and porosity at the interface region in the limit of zero drag.

4.3. Zero drag

In the limit of zero drag, the flow is acoustically controlled. For such flows it is most convenient to write [10]–[12] in characteristic form. Since the nozzling terms play no role away from the interface region, on the τ and ξ (permeation) scales the characteristic equations are

$$\left(\frac{\partial}{\partial\tau} + (U \pm c)\frac{\partial}{\partial\xi}\right)\left(\frac{2c}{\gamma-1} \pm U\right) = U((\gamma-1)U \mp c)c^{-(\gamma+1)/(\gamma-1)}\exp\left(\frac{\Delta S}{\gamma-1}\right)$$

$$+ \frac{c}{\gamma(\gamma-1)}\left(\frac{\partial}{\partial\tau} + (U \pm c)\frac{\partial}{\partial\xi}\right)\Delta S, \qquad [22a, b]$$

where ΔS is the drag related increase in entropy of each gas parcel as it moves through the bed, and is formally given by

$$\Delta S = \int_{\mathscr{P}} \frac{\gamma(\gamma-1)U^2}{P}\,D\tau, \qquad [23]$$

where $\int_{\mathscr{P}} D\tau$ denotes integration along a particle path. Equations [22a, b] describe the progress of right $(U + c)$ and left $(U - c)$ going waves in the gas in both the burn chamber and the bed. In the limit of zero or weak drag, ΔS can be neglected.

In the absence of drag, the right-hand sides of [22a, b] vanish, leaving the standard equations of one-dimensional gas dynamics. The problem that remains is the shock-tube problem (Riemann problem) modified to include an area change (nozzling) between the high-pressure driver gas (burn chamber) and the low-pressure bed (cf. Thompson (1972), p. 423 and Schreier (1982), p. 238). In

the limit that the initial pressure in the burn chamber, P_{r0}, is much greater than the initial pressure of the gas in the bed, P_{b0}, (i.e. $P_{r0} \gg P_{b0}$) we can neglect P_{b0} and the flow is then globally isentropic. The variables

$$\frac{2c}{\gamma - 1} \pm U, \qquad [24a, b]$$

are then constant along the characteristic paths

$$\frac{d\xi}{d\tau} = U \pm c. \qquad [25a, b]$$

The solution then consists of two simple, centered waves (one in the bed, the other in the reservoir) separated by a constant state (in the reservoir) and a P, U-jump through the interface region. With the bed on the right and the reservoir on the left, the solution of this problem is

Bed

$$U = \begin{cases} 0, & \xi > \left(\frac{\gamma+1}{\gamma-1}\right)c_b\tau \\ c_b + \frac{2}{\gamma+1}\frac{\xi}{\tau} & 0 < \xi \leqslant \left(\frac{\gamma+1}{\gamma-1}\right)c_b\tau \end{cases}, \qquad [26]$$

$$c = \begin{cases} 0, & \xi > \left(\frac{\gamma+1}{\gamma-1}\right)c_b\tau \\ c_b - \frac{\gamma-1}{\gamma+1}\frac{\xi}{\tau}, & 0 < \xi \leqslant \left(\frac{\gamma+1}{\gamma-1}\right)c_b\tau \end{cases}, \qquad [27]$$

Reservoir

$$U = \begin{cases} \frac{2}{\gamma-1}(1 - c_r), & \left(\frac{2}{\gamma-1} - \frac{\gamma+1}{\gamma-1}c_r\right)\tau \leqslant \xi < 0 \\ \frac{2}{\gamma+1}\left(1 + \frac{\xi}{\tau}\right), & -\tau \leqslant \xi \leqslant \left(\frac{2}{\gamma-1} - \left(\frac{\gamma+1}{\gamma-1}\right)c_r\right)\tau, \\ 0, & \xi < -\tau \end{cases} \qquad [28]$$

$$c = \begin{cases} c_r, & \left(\frac{2}{\gamma-1} - \frac{\gamma+1}{\gamma-1}c_r\right)\tau \leqslant \xi < 0 \\ \frac{2}{\gamma+1} - \left(\frac{\gamma-1}{\gamma+1}\right)\frac{\xi}{\tau}, & -\tau \leqslant \xi \leqslant \left(\frac{2}{\gamma-1} - \left(\frac{\gamma+1}{\gamma-1}\right)c_r\right)\tau, \\ 1, & \xi < -\tau \end{cases} \qquad [29]$$

where for this case $M_b = 1$ at the "interface" and the constants c_r and c_b are obtained by solving [19] and [21] using the fact that $\psi = (c_b/c_r)^{2/(\gamma-1)}$, $U_b = c_b$ and $U_r = 2(1 - c_r)/(\gamma - 1)$. The numerical solution assuming no drag or heat transfer (two-phase shock tube) is shown in figure 7 for the following parameters: $\phi_G = 0.26$, $P_{r0} = 296$ MPa, $P_{b0} = 0.1$ MPa, $T_{r0} = 4000$ K, and $T_{b0} = 300$ K. The agreement between analytical values on either side of the interface and numerical simulation is good (see figure 7). The numerical calculations utilize MacCormack's method with time splitting to treat the source terms. Importantly, the gas enters the bed at high speed, 1370 m/s for this example, and at a substantial density. Since the zero drag limit describes the early time flow into

the bed, we find that at least initially the penetration rate of the gas into the bed can be high, potentially leading to deep penetration of the bed.

The analysis of the Riemann problem described above shows that as the initial pressure in the bed is increased to a significant fraction of the initial reservoir pressure, eventually $M_b < 1$ which leads to a slower gas flow. Finally, when $P_r = P_b$, the gas flow stops. Up to this point we have ignored the effect of the drag. We show in the next subsection that for typical values of the drag, that (1) the high speed of the first gas to enter the bed is quickly slowed which raises the pressure and that in turn (2) acts to limit the speed of the gas that enters the bed as time goes on.

4.4. Drag interaction

If the high flow velocities of the gas that enters the bed initially continued for times on the order of 10 μs, the penetration of the gas into the bed would be deep (on the order of 1 cm). Differential flow speeds between the solid and gas would then generally represent an important mechanism for transporting mass, momentum and energy in the system. Here we consider two problems that show that the flow speed of the gas decays quickly, leading to low flow speeds at distances $\xi = O(1)$ into the bed. Again we neglect heat transfer. Including heat transfer yields more rapid deceleration of the gas flow.

To gain an understanding of how the drag acts to slow the gas flow, we consider two problems. First we obtain an analytical solution to the problem of an initial small pressure jump in the reservoir relative to the bed. This basically isentropic flow helps us define the structure of the problem and the relative scalings of the variables. Next we do a full numerical simulation of the large pressure jump problem, showing both the early and the late time behavior.

A schematic of the small pressure jump problem is shown in figure 8. Assuming that all the dependent variables can be expanded about the initial reservoir state

$$P = 1 + \epsilon P_1 + \cdots, \quad R = 1 + \epsilon R_1 + \cdots, \quad c = 1 + \epsilon c_1 + \cdots, \quad U = \epsilon U_1 + \cdots, \quad [30a, b, c, d]$$

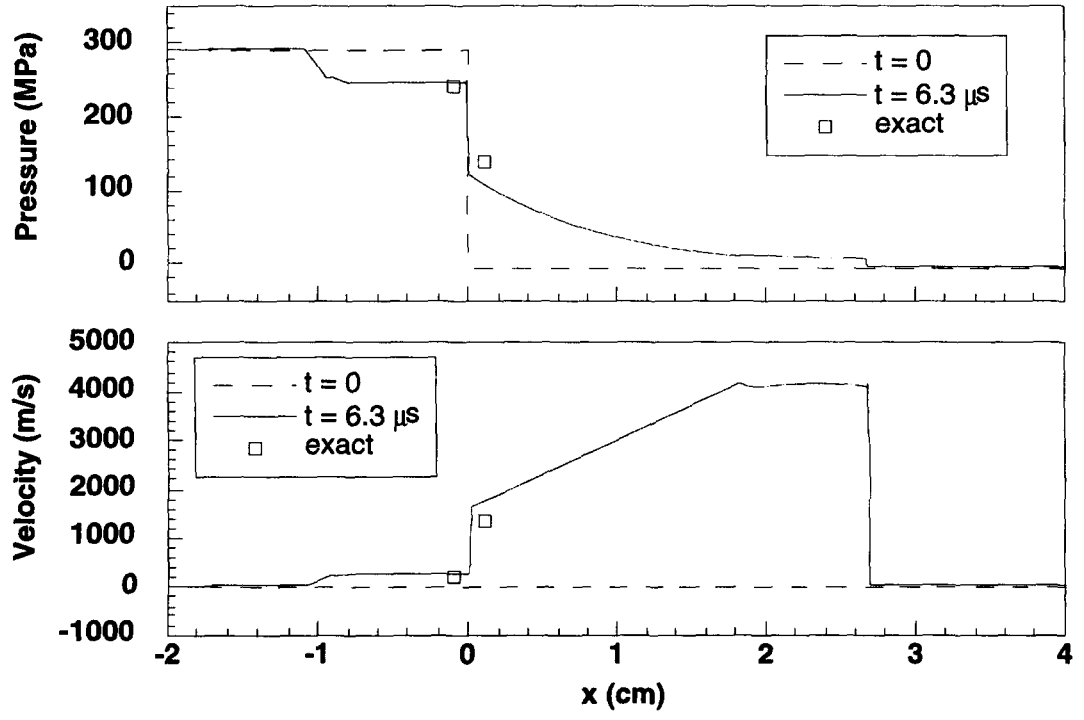

Figure 7. Generalized shock tube simulation and Riemann solution that includes a porosity jump. The grid spacing is $\Delta x = 10$ μm and the interface between the reservoir and bed is 200 μm.

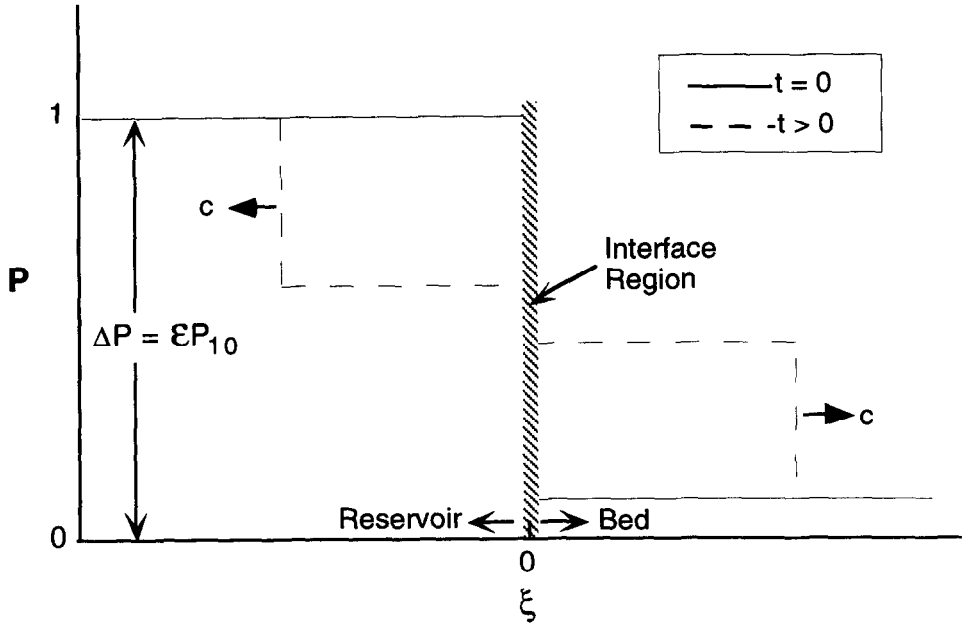

Figure 8. A schematic representation of the small initial pressure jump problem. At $t = 0$ the pressure drops by ϵP_{10} at $\xi = 0$. The zero drag flow that develops for $t > 0$ is also shown. The problem is considered to be infinite in its spatial extent.

where the magnitude of the initial pressure jump $\Delta P \equiv \epsilon P_{10}$ (P_{10} is the initial value of P_1) sets the scale ϵ, then at $O(\epsilon)$ [22a, b] reduce to

$$\left(\frac{\partial}{\partial\tau} \pm \frac{\partial}{\partial\xi}\right)\left(\frac{2c_1}{\gamma - 1} \pm U_1\right) = \mp U_1, \qquad [31a, b]$$

where the drag source term in [31a, b] is only present for $\xi > 0$ (in the bed only).

To help understand the action of the "interface" boundary condition, we first consider the zero drag problem, leading to the result that we have two noninteracting waves

$$\left(\frac{2c_1}{\gamma - 1} + U_1\right) = f(\xi - \tau) \qquad [32]$$

and

$$\left(\frac{2c_1}{\gamma - 1} - U_1\right) = g(\xi + \tau), \qquad [33]$$

where f and g are as yet arbitrary functions and where, for this isentropic flow,

$$P_1 = \frac{2\gamma}{\gamma - 1} c_1. \qquad [34]$$

For this linear, non-interacting wave problem, we have a forward-going wave in the bed and a backward-going wave in the reservoir

Bed

$$\frac{2c_1}{\gamma - 1} + U_1 = f(\xi - \tau), \quad \frac{2c_1}{\gamma - 1} - U_1 = 0, \qquad [35]$$

$$U_1 = \tfrac{1}{2} f(\xi - \tau), \quad P_1 = \frac{\gamma}{2} f(\xi - \tau), \qquad [36]$$

Reservoir

$$\frac{2c_1}{\gamma - 1} - U_1 = g(\xi + \tau), \quad \frac{2c_1}{\gamma - 1} + U_1 = 0, \tag{37}$$

$$U_1 = -\tfrac{1}{2} g(\xi + \tau), \quad P_1 = \frac{\gamma}{2} g(\xi + \tau). \tag{38}$$

Applying the first interface condition, given by [19], yields the condition

$$g(\tau) = -\phi_{Gb} f(-\tau). \tag{39}$$

Applying the second interface condition, given by [21], then yields the final determining condition for this problem

$$\frac{\epsilon^2}{4}(f(-\tau))^2 = \frac{2}{\gamma}\frac{\epsilon}{(1 - \phi_{Gb}^2)}\left\{P_{10} - \frac{\gamma}{2} f(-\tau)(1 + \phi_{Gb})\right\}, \tag{40}$$

where for this flow $M_b^2 \ll 1$. From [40] it is clear that through $O(\epsilon)$ the pressure is continuous and the velocity experiences a jump through the interface region

Bed

$$U = \epsilon \frac{1}{\gamma}\frac{P_{10}}{(1 + \phi_{Gb})}, \tag{41a}$$

$$P = 1 - \epsilon \frac{\phi_{Gb} P_{10}}{(1 + \phi_{Gb})}, \tag{41b}$$

Reservoir

$$U = \epsilon \frac{1}{\gamma}\frac{\phi_{Gb} P_{10}}{(1 + \phi_{Gb})}, \tag{41c}$$

$$P = 1 - \epsilon \frac{\phi_{Gb} P_{10}}{(1 + \phi_{Gb})}. \tag{41d}$$

In fact it follows from [21] that $O(\epsilon^2)$ pressure jumps are associated with $O(\epsilon)$ changes in velocity across the interface region. Thus jumps in porosity tend to produce velocity jumps even for small pressure differentials across the interface region. This is consistent with jumps observed in numerical simulations.

Going on to consider the influence of drag, we now must deal with the coupling between the wave families. Focusing our attention on the bed (since the just completed analysis continues to describe the reservoir) and now define $f \equiv 2c_1/(\gamma - 1) + U_1$, we get

$$\left(\frac{\partial}{\partial \tau} - \frac{\partial}{\partial \xi}\right)\left(\frac{\partial}{\partial \tau} + \frac{\partial}{\partial \xi}\right) f + \frac{\partial f}{\partial \tau} = 0. \tag{42}$$

Equation [42] is called the telegrapher's or damped wave equation. It has the structure of equations that describe a wave hierarchy (see Whitham (1974)). Importantly, for short times the second order operator controls the evolution of the flow, while for late times the control switches to a first order operator. Since our goal is to understand the structure of the flow, we use a simplified asymptotic analysis to expose the properties of [42].

We consider two limits: (1) a short-time, high-frequency, wave head limit, where

$$\xi - \xi_0 \equiv \epsilon x, \quad \tau - \tau_0 \equiv \epsilon t, \tag{43}$$

and (2) a long-time, low-frequency, *far-field* limit, where

$$\xi \equiv \frac{x}{\epsilon}, \quad \tau \equiv \frac{t}{\epsilon}. \tag{44}$$

The limit described by [43] is used to focus in on the evolution of the head of the acoustic wave, while the scaling of [44] is used to examine the flow at several drag scale distances, x_p, into the bed.

In the wave head limit, we find that we have essentially decoupled waves whose amplitude at the wave head decays rapidly with time

$$f = \begin{cases} \mathscr{F}(x - t)\exp(-\epsilon t/2) + \cdots \\ \mathscr{G}(x + t)\exp(-\epsilon t/2) + \cdots \end{cases} \quad [45]$$

Thus the amplitude of the rapidly propagating acoustic-like mode decays exponentially with time on the drag time scale. This says that within a distance x_p of the interface region, the amplitude of the fast wave is inconsequential.

In the far-field limit, we find that [42] behaves asymptotically like a diffusion equation

$$f_t - \epsilon f_{xx} + O(\epsilon^2) = 0. \quad [46]$$

Equation [46] supports a slow, diffusively controlled flow (with A constant)

$$f = A\frac{1}{\sqrt{t}}\exp\left(-\frac{x^2}{4\epsilon t}\right), \quad [47]$$

where at the wave head (with B an $O(1)$ constant)

$$x \sim 2\sqrt{\epsilon t}B, \quad [48]$$

and

$$\frac{d\xi}{d\tau} = \frac{dx}{dt} \sim \sqrt{\epsilon/t}B. \quad [49]$$

Thus at times long compared to t_p, the wave head moves slowly (not at acoustic speeds) and the amplitude decays like $1/\sqrt{t}$. An analysis through $O(\epsilon^2)$ is required to capture a more detailed picture of the small amplitude, slow flow that develops. This is beyond the scope of the present work.

A short-time snapshot of a full numerical simulation of the flow with drag is shown in figure 9. The x–t plot of the pressure field (top of figure) shows the decay of the wave speed entering the bed. This is evident by the change in slope of the contours in the bed with time. Again, heat transfer has been neglected in this simulation and except for the drag interaction, the simulation is the same as shown in figure 7. The slowness of the drag-controlled flow is evident by the factor of 10 reduction in the spatial scales required to represent this case relative to the zero drag flow (compare with figure 7). The flow speed is down to near 200 m/s after 4 μs of flow in a $\phi_{Gb} = 0.26$ porosity bed. Assuming a Reynold's number dependent drag coefficient yields even faster deceleration. If heat transfer is included, the deceleration is slightly faster. A full simulation with both a Reynold's number dependent drag coefficient and heat transfer is considered later.

Another interesting feature of this simulation is that extremely high gas temperatures ($>10{,}000$ K) are observed at the head of the wave front. These high temperatures are a result of drag dissipation. If heat transfer is allowed, more realistic temperatures result (~ 6500 K). Clearly dissipation as a result of flow drag is significant. This fact is also seen in the rational derivation of the low-speed equation under adiabatic conditions (see the appendix).

Measured on the permeation scale, $x_p = 3 \times 10^{-4}$ m, the velocity is down by a factor of 10 from its initial value after the permeation wave has traveled a distance of 10 x_p. Since the pressure gauges used to experimentally measure the "quasi-steady" permeation rate are many times this distance into the bed, we anticipate that the flow at the gauges in the bed will be slow. In the next subsection, we derive the slow flow approximation to [10]–[12].

4.5. Low-speed approximation

The essence of the slow flow approximation is that the inertial terms in [11] can be neglected. This is justified if the acoustic speed is much greater than the convective speed, $|u_G| \ll |c_G^0|$. This approximation is commonly made in the analysis of transient gas flow in porous media. Isothermal and isentropic limits have been considered in previous work (cf. Morrison 1972; Morrison 1976; Morrison 1977; Nilson 1981). Negligible heat transfer between the solid and gas (adiabatic), or very

large heat transfer (isothermal) bracket the actual conditions. The isentropic limit would be appropriate if there is negligible heat transfer *and* drag interaction heating. In other words, if there is negligible heat transfer and drag interaction there are no irreversible terms and consequently no change in entropy can occur within the slow speed approximation. For example, using the isentropic relationship between pressure and density in the mass equation and eliminating u_G by utilizing the low-speed limit of the momentum equation, $\partial P_G/\partial x = -\delta u_G/\phi_G$, yields

$$\frac{\partial}{\partial t}(P_G^{1/\gamma}) - \frac{\partial}{\partial x}\left(\left(\frac{\phi_G}{\delta}\right)P_G^{1/\gamma}\frac{\partial P_G}{\partial x}\right) = 0. \qquad [50]$$

Similar equations can be obtained for the isothermal case (simply let $\gamma \to 1$ in [50]). The resulting equation is a nonlinear diffusion equation. Because of the nonlinearity, this equation has some interesting properties. In particular, the permeation exhibits a discontinuity in the gradient of pressure at the head of the permeation front. Linear diffusion does not produce such discontinuities.

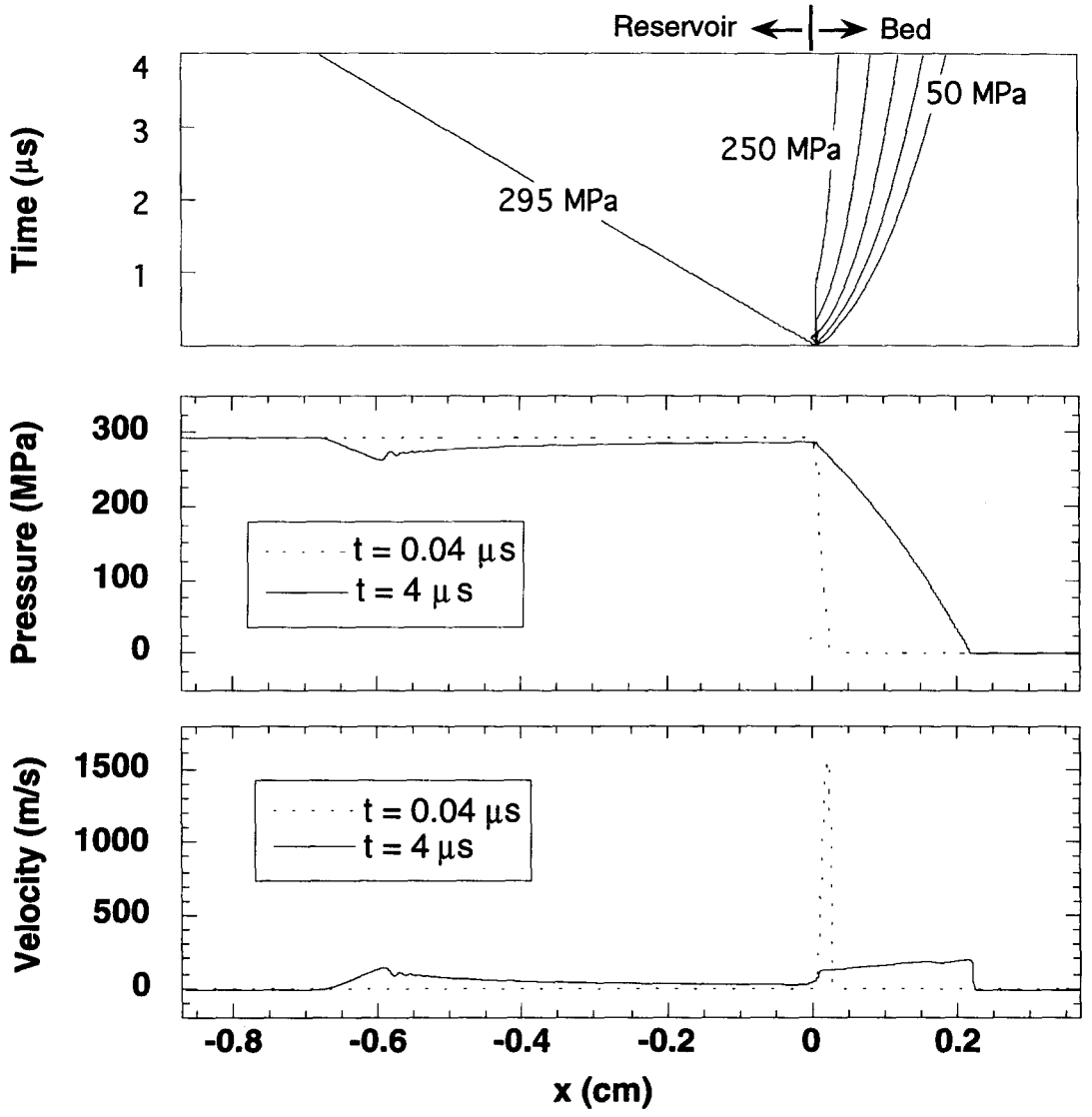

Figure 9. Generalized shock tube simulation with a porosity jump and drag interaction. The pressure contours show the deceleration of the initial wave front into the bed. Profiles of velocity and pressure are also shown. A constant drag coefficient was assumed, $\delta = 2 \times 10^8$ kg/m^3 s. The grid spacing is $\Delta x = 10\ \mu$m and the interface between the reservoir and bed is 200 μm.

Previous workers have assumed that in the low speed approximation the drag dissipation term is negligible (cf. Morrison 1972; Morrison 1976; Morrison 1977; Nilson 1981). As a consequence of this assumption, the isentropic limit results if, in addition, adiabatic conditions are assumed. However, a rational derivation shows that the drag dissipation term cannot be neglected based on the low-speed assumption. We present a rational derivation of the slow-flow equations under adiabatic conditions in the appendix.

The previously derived "jump conditions" across the interface region, [19] and [21] could be used to define the interface boundary condition for a slow-flow equation such as [50] for times larger than t_p so the slow-flow assumptions near the interface will not be violated. These boundary conditions relate P_b, U_b to P_r, when $U_b = -1/\gamma(\partial P_b/\partial\zeta)$ at the interface. An alternative is to use the first experimental gauge in the bed as the left boundary. This avoids the complexities at the interface altogether.

4.6. *Estimate of drag coefficient directly from data*

It is useful to derive a simple relationship between the measured pressure traces (measured at a fixed point), the drag coefficient (δ), and permeation rate (u_G). We begin by rewriting the mass equation, [2a], for the gas phase in the bed,

$$\frac{\partial \rho_G}{\partial t} + u_G \frac{\partial \rho_G}{\partial x} + \rho_G \frac{\partial u_G}{\partial x} = 0. \qquad [51]$$

Just behind the head of the permeation wave $\rho_G = 0$ and $p_G = 0$ (see figure 9 for example) so that we drop the last term in [51]. Further, if there is a simple relationship between density and pressure such as $\rho_G = f(p_G)$ it follows that replacing density by pressure in this reduced mass equation gives,

$$\left.\frac{\partial p_G}{\partial t}\right|_{p_G<\Delta p_G} = -u_G \left.\frac{\partial p_G}{\partial x}\right|_{p_G<\Delta p_G}, \qquad [52]$$

where the restriction $p_G < \Delta p_G$ has been explicitly noted to indicate that the relationship is applied at the wave head where the pressure is just above the initial very low gas pressure in the bed. At the wave head the gas momentum equation simplifies to $\partial p_G/\partial x = -\delta u_G/\phi_G$ (negligible inertial terms in low gas density regions). Using this simplified momentum equation in [52] yields

$$\delta = \left.\frac{\phi_G}{u_G^2}\frac{\partial p_G}{\partial t}\right|_{p_G<\Delta p_G}. \qquad [53]$$

This expression provides a simple relationship between the drag coefficient, measured pressure traces (measured at a fixed point), and permeation rate (estimated from arrival times of the permeation wave). This relationship is useful in obtaining direct estimates of δ from the experimental data. Note that no additional assumptions are made concerning the heat transfer or speed of the flow in the derivation of this expression. The utility of this expression is demonstrated in the results section.

5. ANALYSIS OF EXPERIMENTS

In this section the data are presented and models described in the previous sections are compared with experiments. The most direct result from the data is the macroscopic permeation rate as a function of the maximum reservoir pressure. The macroscopic permeation rate was obtained from the initial rise reported by the three pressure gauges in the bed. Figure 10 shows the measured permeation rate as a function of reservoir pressure for the three experiments (the trivial result of equal reservoir and bed pressure with no flow is also plotted). The maximum permeation rate obtained in these tests is only 6.5 m/s for the 621 MPa case. This is at least an order of magnitude below the propagation rate sometimes attributed to convective burning in energetic materials.

It is not likely that driving pressures in convective burning of energetic materials could be significantly higher than the maximum pressure considered here (621 MPa). These data also

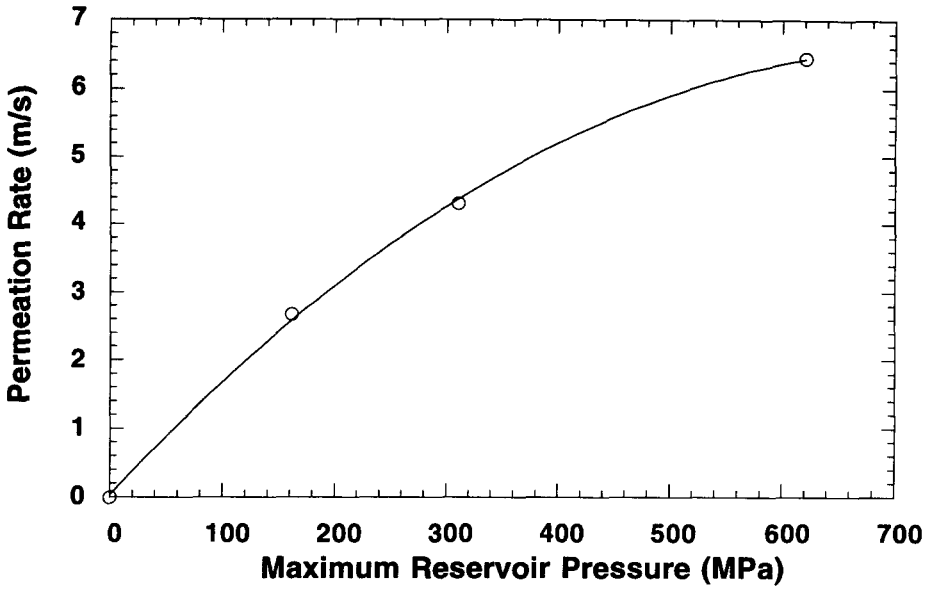

Figure 10. Measured macroscopic permeation rate as a function of maximum reservoir pressure. A curve fit of the data is shown.

indicate that the permeation rate has a decreasing sensitivity to driving (reservoir) pressure as the pressure increases (see figure 10). This trend is consistent with drag coefficients (see [1]) that generally exhibit an increase in the drag coefficient with permeation rate. Therefore, even if driving pressures were increased significantly above the pressures considered here, it appears nearly impossible to attain macroscopic permeation rates an order of magnitude higher than those reported for this porous system.

These results indicate that the commonly accepted mechanism of *deep*, rapidly penetrating hot gases preheating material to ignition is not physically plausible for the conditions considered. However, a form of convective burning is experimentally observed under some conditions. A modified physical picture is discussed later.

5.1. Numerical simulation

A full simulation of one of the experiments, including heat transfer and acoustic time scales, was made. The equations were integrated numerically as previously described. An initial step in pressure was assumed; that is, the reservoir is assumed to be pressurized instantaneously. In the experiments the pressurization in the reservoir is rapid, so this is a reasonable approximation (see figure 6). The maximum reservoir pressure was 310 MPa, which corresponds to the intermediate pressure considered. The drag and heat transfer were modeled using a correlation by Gel'Perin & Ainstein (1971),

$$H = \frac{3\phi_S k_G}{a^2}(1 - 0.2\mathrm{Re}^{2/3}\mathrm{Pr}^{1/3}). \qquad [54]$$

The Prandtl number, Pr, was assumed to be 0.75, and a is the particle radius. The following drag law was assumed as a function of the Reynolds number, Re ($\equiv 2\phi_S\rho_S a u_G/\mu_G$):

$$\delta = \frac{\mu_G}{\kappa}\left(1 + \frac{\varsigma_1 \mathrm{Re}}{\phi_S}\right). \qquad [55]$$

The conductivity, k_G, and the viscosity, μ_G, of the gas were assumed to be 7.0×10^{-2} W/m K and 5.0×10^{-5} kg/m s, respectively. The permeability, κ, is given by

$$\kappa = \frac{4a^2\phi_G^{4.5}}{\varsigma_2}. \qquad [56]$$

Here ς_1 and ς_2 are empirical constants. The values used by Baer & Nunziato (1986) were adopted ($\varsigma_1 = 0.01$ and $\varsigma_2 = 33$). These values are shown later, based on these experiments, to produce reasonable values for the drag coefficient.

Figure 11 shows the results of this calculation. The Reynolds number drag coefficient quickly slows the flow near the interface (compare with part (a) of figure 11 with top of figure 9). A constant drag coefficient will overpredict the permeation rate. We also observe that the gas is rapidly cooled to near ambient temperature in a very short distance (see part (b) of figure 11). For this simulation after 1 ms, the gas has penetrated about 1 cm, while the temperature has dropped to 400 K 3 mm

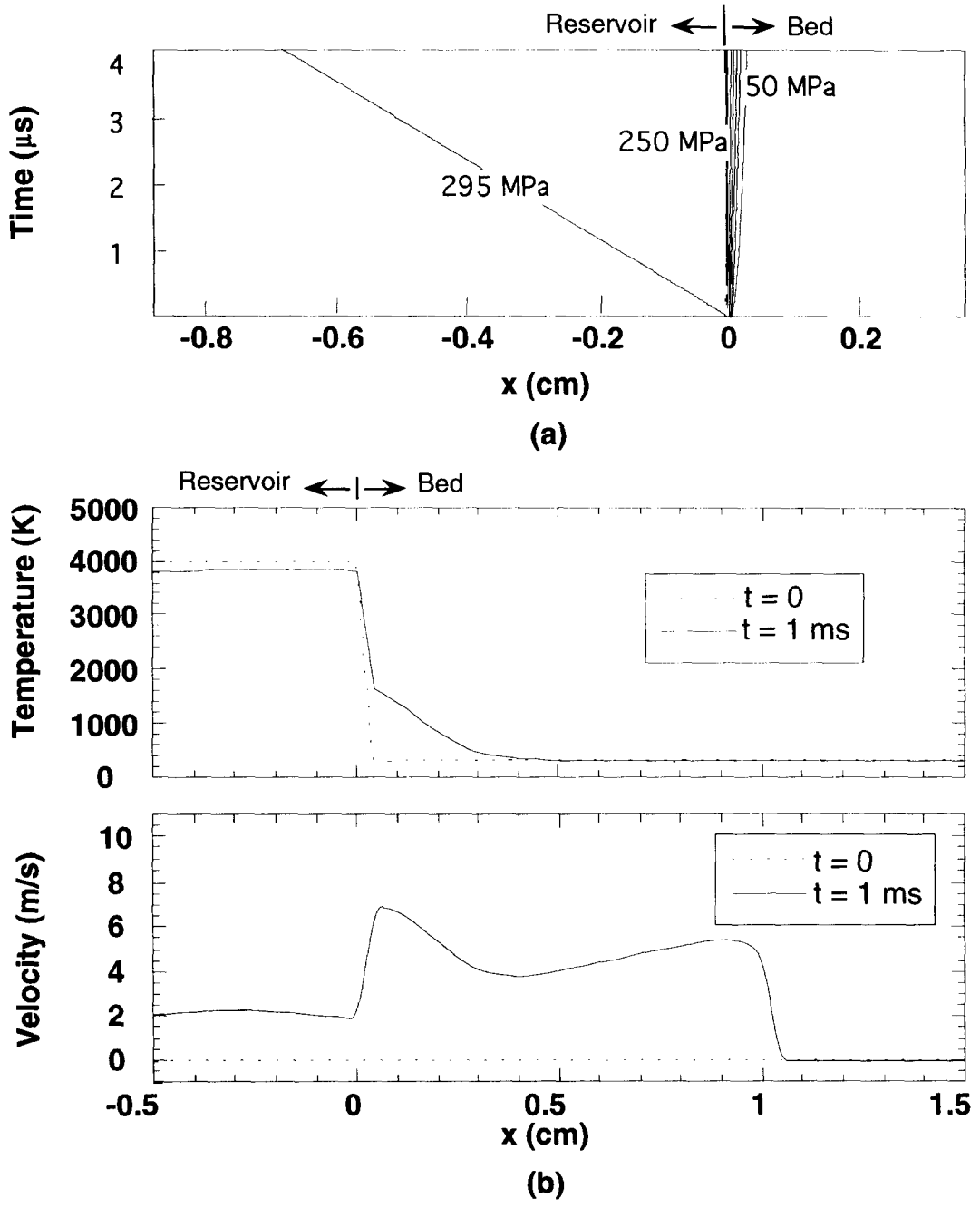

Figure 11. Full simulation of an experiment including flow-dependent heat transfer and drag interaction. Pressure contours show the rapid deceleration of the initial wave front into the bed at early times (compare with figure 9). Profiles of velocity and temperature are also shown. The grid spacing is $\Delta x = 10$ μm and the interface between the reservoir and bed is 200 μm.

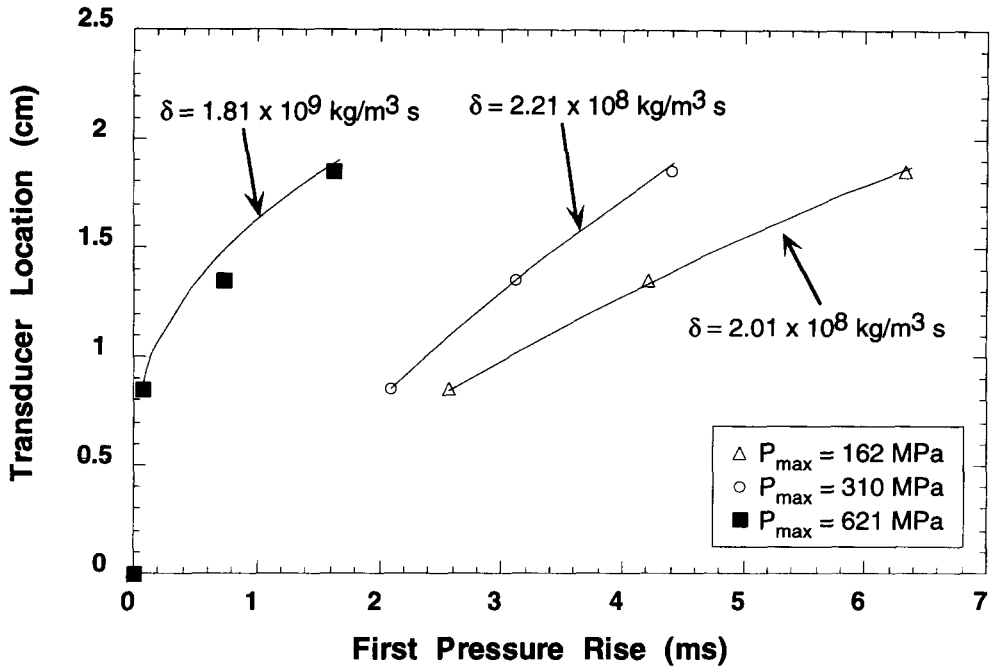

Figure 12. Measured transducer location as a function of first pressure rise (x–t plot) compared with simplified isothermal calculations.

from the interface region. Therefore, an isothermal flow in the bed can be reasonably assumed for these experiments. Furthermore, the simulation shows (see part (b) of figure 11) that the permeation rate in the bed is about 5.5 m/s after 1 ms which is reasonably close to the measured permeation rate of 4.2 m/s for this same case at a later time. The predicted arrival time to the first gauge in the bed also compares reasonably well with experiment (in the simulation the arrival time is 0.9 ms at the first gauge in the bed compared to about 1 ms in the experiment). At early times the speed of the gas is large in the interface region. As a consequence, the heat transfer is very rapid at early times also. Because this permeation rate is much less than the gas sound speed, the low-speed approximation applied to the flow in the bed away from the interface can be expected to be a reasonable approximation as well. In these simulations the permeation rate is only large very near the interface region between the bed and the reservoir at very early times.

5.2. Comparison of data with isothermal low-speed flow calculations

Assuming low speed flow and isothermal conditions, [50] (with $\gamma \to 1$) can be numerically integrated. Other heat transfer conditions, such as adiabatic conditions, could be specified. However, it turns out that determination of the drag coefficient is insensitive to the heat transfer assumed. A standard IMSL† library PDE solver (DPDES) was used to integrate the equations. A constant drag coefficient for each case was assumed, and optimal fits to the data were made to obtain an effective drag coefficient for each case. The results of these calculations are shown in figure 12 for the three experimental cases. Figure 12 is an x–t plot of the locations of the first rise in pressure. The first gauge in the bed provided the left boundary condition for the simulation. This approach avoided the complexities involved at the interface. Further, assumptions made in the simplified analysis (low speed) are justified in the bed away from the interface region.

The drag coefficients obtained from this analysis are large. This is consistent with the observation that the macroscopic permeation rate is small even though the driving pressure difference is substantial. Figure 13 shows a typical comparison between the calculated pressure traces (using [50] with $\gamma \to 1$) and the measurements. The shapes in the pressure traces are reproduced well using this simplified model. Better agreement could possibly be achieved by relaxing the isothermal

†International Mathematical and Statistical Libraries, Inc., Houston, TX.

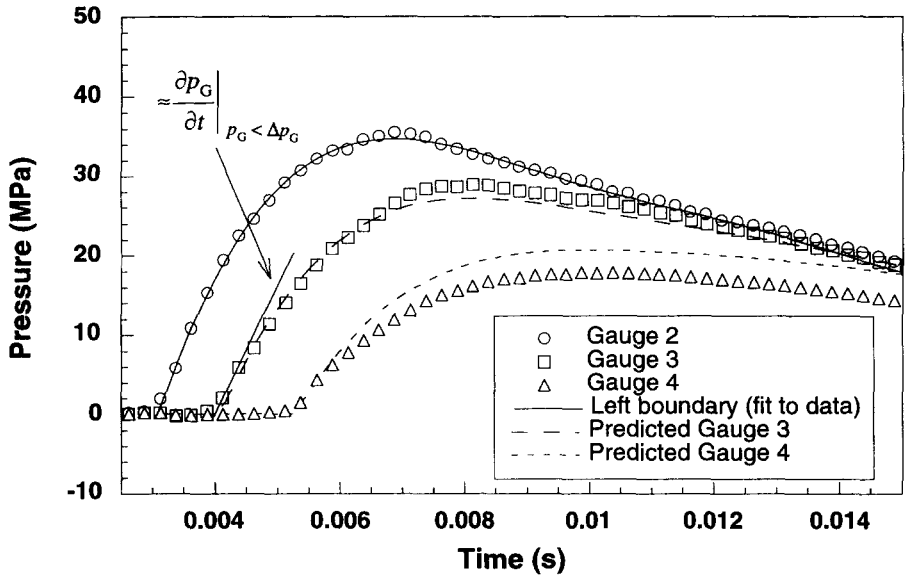

Figure 13. Representative measured pressure traces in granular bed compared with simplified isothermal calculations (see [50]).

assumption or assuming a nonconstant form of the drag coefficient (i.e. include velocity and density dependency). However, this simple model is adequate to establish the magnitude of the drag coefficient and support the conclusions of this work.

As described previously, the drag coefficient can also be obtained directly from the experimental record. In particular, [53] can be applied to the data record. An estimate of the rate of pressurization at the wave head ($\partial p_G/\partial t|_{p_G<\Delta p_G}$) can be obtained from the pressure trace of the middle gauge in the bed, gauge 3 (see figure 13). The arrival times of the permeation wave can be used to obtain an estimate of the permeation rate and then [53] can be evaluated. These directly calculated drag coefficients are presented in figure 14. The drag coefficients obtained from fitting the low-speed calculations to the data are also shown for comparison. The measured drag coefficient for the highest permeation rate (highest maximum reservoir pressure) considered is significantly larger than

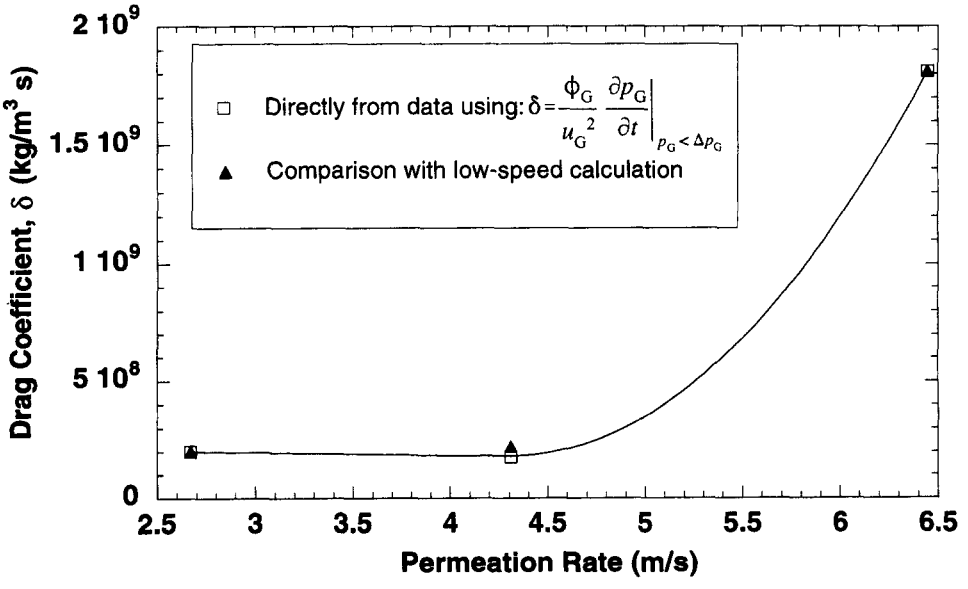

Figure 14. Measured drag coefficient as a function of permeation rate. A curve fit of the measurements is shown.

for the lower permeation rates (lower reservoir pressures). This trend is consistent with the Forchheimer equation, [1], that shows that as density (or pressure) and permeation rate increase, the drag coefficient increases.

Neglecting the inertial term (second term of the Forchheimer equation) we can obtain an estimate of the permeability,

$$\kappa = \frac{\mu_G}{\delta}. \qquad [57]$$

For the lower permeation rates measured, the drag coefficient, δ, is about 2.0×10^8 kg/m^3 s. Assuming $\mu_G = 5.0 \times 10^{-5}$ kg/m s the permeability, κ, is about 2.5×10^{-13} m^2. This permeability is lower (higher drag coefficient) than correlations based on spherical particles. For example, using the Carman–Kozeny expression (MacDonald *et al.* 1979) for permeability we get $\kappa = 6.0 \times 10^{-13}$ m^2 which is larger than the measured permeability. Other commonly used spherical-particle correlations predict even higher permeabilities. Lower permeabilities are expected for complex shaped particles since the flow path is more tortuous.

These results compare well with correlations made in similar materials at lower pressures. For example, using the parameters assumed by Baer & Nunziato (1986) which are based on measurements made by Shepherd & Begeal (1988) we estimate the permeability to be 2.4×10^{-13} m^2 compared to 2.5×10^{-13} m^2 measured here (only a 4% difference). These results indicate that permeabilities do not change in unexpected ways in experiments driven with high reservoir pressures.

6. RELEVANCE TO CONVECTIVE BURNING

Our experiments were designed to measure the permeability of a granular bed when it is subjected to an applied pressure jump at one end. We saw that a large initial pressure drop across the interface region leads to a very high initial flow speed into the bed. These dynamics were controlled by [20]. However, the porous bed combustion problems of principal interest are *wave* problems, where the "interface" moves relative to the solid bed. An equation similar to [20] can also be derived in a reference frame attached to a steadily propagating compaction wave

$$\frac{dM^2}{d\zeta} = M^2\left\{\frac{(\gamma - 1)M^2 + 2}{M^2 - 1}\right\}\left(\frac{1}{\phi_G}\right)\frac{d\phi_G}{d\zeta}, \qquad [58]$$

where $M^2 \Rightarrow (u_G - D)^2/c_G^2$, D is the wave speed, $\zeta = 0$ at the wave head with $\zeta > 0$ in the undisturbed material. In deriving [58] we have assumed that compaction work goes exclusively to the solid. In the region where the solid has been compacted (i.e. $\zeta \leq 0$), u_G is generally some significant fraction of D with $u_G \leq D$. From [58] we learn that the porosity gradient, $d\phi_G/d\zeta \geq 0$ associated with a compaction wave moving towards $\zeta > 0$, acts as a nozzle that can drive changes in u_G in the direction of increasing ζ. Here we argue that the maximum gas velocity projected ahead of the compaction wave is D.

When D is of the order of the sound speed in the undisturbed gas (a typical situation), then in the region where the solid is compacted $M^2 < 1$ in the gas since u_G is some fraction of D. Therefore, from [58] it follows that $dM^2/d\zeta < 0$ and the moving interface (compaction wave) drives $M^2 \to 0$ (i.e. making $u_G = D$ in the region ahead of the compaction wave). Thus the dynamics of the interface *do not* propel gas ahead of a compaction wave. This situation is analogous to a diverging nozzle. The decrease in the porosity produced by the compaction wave acts like an interface that is a virtual piston which leads to a gas phase wave of speed $D + c_{G0,b}$, where $c_{G0,b}$ is the sound speed in the undisturbed gas. The typical speed we would see here is of the order of 500 m/s. The drag forces that we have measured would quickly reduce any such permeation wave to zero. Making the sound speed in the undisturbed gas greater (the situation if the material ahead of the wave were partially burned) will not change this conclusion. When $c_{G0,b}$ and c_G are sufficiently less than D, then $M^2 > 1$ in the compacted region, and [58] leads to u_G being *reduced* in the direction of the uncompacted solid. Thus, in this case, permeation is a moot point since there is no driving force to generate gas flow which is faster than the speed of the interface. These results on moving

interfaces (specifically compaction waves) along with the large drag coefficients that we found, make it highly unlikely that gas could permeate a significant distance ahead of this type of moving front. However, there are other conditions that also may be of interest.

Compaction is severely inhibited in some experiments (e.g. Fifer & Cole 1981) used to study convective burning in which a granular explosive is loosely confined and placed in a large volume Crawford bomb. Such experiments yield a favorable nozzling effect ($d\phi_G/d\zeta \leqslant 0$) behind the ignition front for permeation since decompaction occurs. The nozzling effect would accelerate the gas flow, as it does in the transient permeation experiment studied here. Under possible accident conditions damaged explosives are likely to be more confined. Under more confinement there would be no release to a nearly constant pressure as in the Crawford bomb. Consequently, pressure would rapidly build, yielding a compaction wave into the damaged explosive. When compaction occurs, high speed permeation becomes unlikely, as discussed above. The compaction dissipates energy by such processes as friction between particles and visco-plastic work and is driven by increasing pressures behind the wave. Thus, compaction provides an alternative mode of propagating energy forward. Still, convective burning may potentially be an important mechanism at very early times before compaction processes begin if burning is thermally initiated. However, in strong confinement it is likely that burning very quickly yields compaction waves that inhibit convective burning. If compaction processes initiate reaction, permeation probably does not play an important role.

The results reported in this paper show that drag coefficients are very large in low-porosity ($\phi_G \leqslant 0.3$) granular material. A high drag coefficient corresponds to a very thin permeation layer (where the solid and gas speeds are not equal) ahead of the ignition front in a convective combustion wave. A thin permeation scale will yield a different wave structure than commonly assumed. Consequently, interpretations and conclusions of previous work will be affected. For example, Drew's (1986) approximate solutions of convective burning (no compaction) showed that thermal conductivity plays a leading role in the determination of the propagation rate, and a propagation speed that is relatively insensitive to interphase heat transfer and drag. Drew's approximate solution also yields propagation rates that are lower than experimentally observed. An important point is that Drew's conclusions are based on analysis based on a *specified* structure that includes *deep* permeation of the hot gases into the bed ahead of the ignition front. If the drag interaction is significantly different than commonly assumed, the structure (the permeation length scale) would change drastically and the conclusions based on the previous physical picture could be irrelevant. Our results suggest a much thinner permeation structure. As a consequence, the permeation layer may then influence the propagation rate significantly. Higher propagation rates are possible because convective heat transfer can potentially transport energy forward faster than diffusion. Gol'dshtein *et al.* (1994) recently considered flame propagation via barodiffusivity (permeation) only and showed by approximate analysis that the mechanism is possible. However, the approximate analysis of Gol'dshtein *et al.* is heuristic and merits a more detailed study.

A significantly different physical picture of convective burning can be postulated based on our work. To sustain a very rapid convective wave, energy must be transported forward rapidly by convection through a thin permeation layer. To overcome the large resistance posed by the large drag coefficients, a steep pressure gradient is necessary to sustain this permeation. A large pressure gradient can be sustained near the ignition region when sufficiently rapid burning occurs within the granular bed due to the confinement between particles (large effective drag coefficients). It is easily shown that the burning of very small amounts of explosive yields high pressures under such confined conditions. For example, simple estimates show that burning a 1 μm shell yields pressures on the order of 100 MPa in a 50 μm spherical hole in HMX. Therefore, the rate of reaction does not have to be extraordinarily high to promptly increase pressures. Further, the confinement would be largely maintained with only a small amount of solid converted to gas. The resulting pressure gradients would drive rapid permeation through *thin* regions ahead of the ignition point into the next layers of undisturbed particles.

For this mechanism to exist, burning must occur *within* the bed. When the standoff distance of the gas phase flame is larger than the pore size, the flame *can not* spread into the bed since gas phase reaction is quenched by the cool particles, as postulated in the Russian literature (cf. Ermolaev *et al.* 1975). The standoff distance decreases with pressure. At a critical pressure the standoff distance is sufficiently small that burning can occur in the granular bed. Convective burning experiments, where

compaction is inhibited, have exhibited rapid ejection of particles from the particle bed (cf. Fifer & Cole 1981). This implies a significant pressure rise in the wave with expansion into the large volume. This observation is consistent with the picture proposed here. However, a complete study of this postulated structure, including a study of the competing drag and reaction time scales, is beyond the scope of this study.

Another implication of these results is that the asymptotic large-drag limit of full two-phase equations may be justifiable under many conditions, which is a significant simplification. Motivated by our experimental results, the large drag limit of full two phase equations has been considered recently (Bdzil *et al.* 1996c). The equations resulting from a large drag limit applied to a two-phase, two-velocity model have two favorable properties. First, the extremely narrow spatial scale associated with velocity equilibration does not have to be resolved. Accurate numerical results from the full two-velocity equations must resolve this very thin scale both spatially and temporally to get the proper momentum transfer between the phases. This presents serious numerical difficulties. Second, the equations have only a single bulk velocity. This simplifies the task of implementing such models in current multi-dimensional, multi-material hydrocodes that generally evolve only one velocity field as well as implementation of boundary conditions (Kober *et al.* 1995; Son *et al.* 1995). This large drag limit has been further justified in simulations of piston-initiated DDT by favorable comparisons between full two-velocity and the large drag model simulations (Bdzil *et al.* 1996c). These issues are discussed in more detail elsewhere (Bdzil & Son 1995; Bdzil *et al.* 1996c; Bdzil *et al.* 1996b; Bdzil *et al.* 1996a).

7. CONCLUSIONS

From this work we make the following major conclusions: (1) The results indicate that rapid and *deep* penetration of hot gases (many particle diameters) at high velocities does not occur for the conditions considered. Generally the porosity in damaged explosives is expected to be less than 30% porosity studied here. Consequently, the conditions studied can be considered a worst-case for problems of interest. The measured permeability is consistent with lower pressure results in similar materials, but is significantly lower than predicted by correlations based on beds of spherical particles. (2) In these experiments rapid flow occurs near the interface region for short times, but is quickly decelerated. (3) The convective burning wave structure, when conditions allow its occurrence, will be significantly different than commonly postulated. In particular, a much thinner permeation layer than typically assumed is expected to occur. This is expected to change the conclusions arising from combustion analyses that assume a thick permeation layer. (4) When the low-speed permeation approximation is rationally derived assuming adiabatic conditions, drag dissipation cannot be neglected as commonly assumed. (5) The presence of a compaction wave will inhibit rapid permeation; analogous to a diverging nozzle for subsonic flow. Consequently, compaction processes likely play a more significant role in DDT than generally assumed. However, under special conditions (compaction-inhibited experiments or early times in a thermally ignited granular bed) convective burning can potentially still play a role. This should be further investigated. (6) An asymptotic limit of two-phase two-velocity models is justifiable for many cases of interest and may significantly simplify DDT modeling.

Acknowledgements—The authors would like to acknowledge support for this work from Los Alamos National Laboratory which is supported by the U. S. Department of Energy under contract number W-7405-ENG-36. Gary Laabs was responsible for fielding the convective flow experiments. Contributions by John McAfee, Bill Davis, Scott Stewart, and Ash Kapila are also acknowledged.

REFERENCES

Akhatov, I. S. & Vainshtein, P. B. 1983 Transition of porous explosive combustion into detonation. *Fizika Goreniya i Vzryva* **20,** 70–77.

Andreev, K. K. & Chuiko, S. V. 1963 Transition of the burning of explosives into an explosion. I. Burning of powdered explosives at constant high pressures. *Russian Journal of Physical Chemistry* **37,** 695–699.

Baer, M. R. & Nunziato, J. W. 1986 A two-phase mixture theory for the deflagration-to-detonation transition (DDT) in reactive granular materials. *International Journal of Multiphase Flow* **12,** 861–889.

Bdzil, J. B., Kapila, A., Menikoff, R., Son, S. F. & Stewart, D. S. 1996a Structure of the velocity relaxation zone in the Baer-Nunziato model (in preparation).

Bdzil, J. B., Kapila, A., Menikoff, R., Son, S. F. & Stewart, D. S. 1996b Towards a new two-phase model of DDT—Part I: Review of modeling issues (in preparation).

Bdzil, J. B., Kapila, A., Menikoff, R., Son, S. F. & Stewart, D. S. 1996c Towards a new two-phase model of DDT—Part II: Reduced models and numerical simulations (in preparation).

Bdzil, J. B. & Son, S. F. 1995 *Engineering Models of Deflagration-to-Detonation Transition*. Los Alamos National Laboratory, LA-12794-MS.

Belyaev, A. F., Bobolev, V. K., Korotkov, A. I., Sulimov, A. A. & Chuiko, S. V. 1975 *Transition From Deflagration to Detonation in Condensed Phases*. Jerusalem, Israel Program for Scientific Translations.

Belyaev, A. F., Korotkov, A. I., & Sulimov, A. A. 1966 Breakdown of surface burning of gas-permeable porous systems. *Fizika Goreniya i Vzryva* **2,** 47–58.

Bernecker, R. R. 1986 The deflagration-to-detonation transition process for high-energy propellants—a review. *AIAA Journal* **24,** 82–91.

Bernecker, R. R. & Price, D. 1974a Studies in the transition from deflagration to detonation in granular explosives—I. Experimental arrangement and behavior of explosives which fail to exhibit detonation. *Combustion and Flame* **22,** 111–117.

Bernecker, R. R. & Price, D. 1974b Studies in the transition from deflagration to detonation in granular explosives—II. Transitional characteristics and mechanisms observed in 91/9 RDX/WAX. *Combustion and Flame* **22,** 119–129.

Bernecker, R. R. & Price, D. 1974c Studies in the transition from deflagration to detonation in granular explosives—III. Proposed mechanisms for transition and comparison with other proposals in the literature. *Combustion and Flame* **22,** 161–170.

Bobolev, V. K., Margolin, A. D. & Chuiko, S. V. 1966 Stability of normal burning of porous systems at constant pressure. *Fizika Goreniya i Vzryva* **2,** 24–32.

Drew, D. A. 1986 One-dimensional burning wave in a bed of monopropellant particles. *Combust. Sci. and Tech.* **47,** 139–164.

Dubovitskii, V. F., Korostelev, V. G., Korotkov, A. I., Frolov, Y. V., Firsov, A. N., Shkadinskii, K. G. & Khomik, S. V. 1974 Burning of porous condensed systems and powders. *Fizika Goreniya i Vzryva* **10,** 811–818.

Ermolaev, B. S., Khasainov, B. A., Borisov, A. A. & Korotkov, A. I. 1975 Convective combustion propagation in porous low and high explosives. *Fizika Goreniya i Vzryva* **11,** 720–730.

Fifer, R. A. & Cole, J. E. 1981 Transitions from laminar burning for porous crystalline explosives. In *Seventh Symposium (International) on Detonation*, Annapolis, MD, Office of Naval Research, Department of the Navy.

Forchheimer, P. H. Z. 1901 *Ver. Deursch. Ing.* **45.**

Gel'Perin, N. I. & Ainstein, V. G. 1971 Heat transfer in fluidized beds. In *Fluidization*. Academic Press, New York.

Gockhale, S. S. & Krier, H. 1982 Modeling of unsteady two-phase reactive flow in porous beds of propellant. *Progress in Energy and Combustion Science* **8,** 1–39.

Gol'dshtein, V., Shreiber, I. & Sivashinsky, G. 1994 On creeping detonation of filtration combustion. *Shock Waves* **4,** 109–112.

Griffiths, N. & Groocock, J. M. 1960 The burning to detonation of solid explosives. *Journal Chemical Society of London* **814,** 4154–4162.

Kober, E. M., Bdzil, J. B. & Son, S. F. 1995 Modeling DDT in granular explosives with a multi-dimensional hydrocode. In *1995 APS Topical Conference on Shock Compression of Condensed Matter*, August 13–18, Seattle, WA.

Korotkov, A. I., Sulimov, A. A., Obmenin, A. V., Dubovitskii, V. F. & Kurkin, A. I. 1969 Transition from combustion to detonation in porous explosives. *Fizika Goreniya i Vzryva* **5,** 315–325.

Krier, H., Rajan, S. & Tassell, W. F. V. 1976 Flame-spreading and combustion in packed beds of propellant grains. *AIAA Journal* **14,** 301–309.

Kuo, K. K., Koo, J. H., Davis, T. R. & Coates, G. R. 1976 Transient combustion in mobile gas-permeable propellants. *Acta Astronautica* **3,** 573–591.

Kuo, K. K. & Summerfield, M. 1974 Theory of steady-state burning of gas-permeable propellants. *AIAA Journal* **12,** 49–56.

Kuo, K. K., Vichnevetsky, R. & Summerfield, M. 1973 Theory of flame front propagation in porous propellant charges under confinement. *AIAA Journal* **11,** 444–451.

MacDonald, I. F., El-Sayed, M. S., Mow, K. & Dullien, F. A. L. 1979 Flow through porous media—the Ergun equation revisited. *Ind. Eng. Chem. Fundam.* **18,** 199–208.

Morrison, F. A. J. 1972 Transient gas flow in a porous column. *I/EC Fundamentals* **11,** 191–197.

Morrison, F. A. J. 1976 Similarity in transient non-Darcy gas flow in a finite porous bed. *ASME Journal of Fluids Engineering* **99,** 191–197.

Morrison, F. A. J. 1977 Similarity in transient high speed gas flow through porous media. *ASME Journal of Fluids Engineering* **38,** 779–781.

Nilson, R. H. 1981 Transient fluid flow in porous media: inertia-dominated to viscous-dominated transition. *Journal of Fluids Engineering* **103,** 339–343.

Obmenin, A. V., Korotkov, A. I., Sulimov, A. A. & Dubovitskii, V. F. 1969 Propagation of predetonation regimes in porous explosives. *Fizika Goreniya i Vzryva* **5,** 461–470.

Pozhariskii, A. N. & Ivanov, A. G. 1993 Explosive initiation of fast convective combustion in a closed volume. *Fizika Goreniya i Vzryva* **29,** 104–110.

Schreier, S. 1982 *Compressible Flow*. New York, Wiley.

Shepherd, J. E. & Begeal, D. R. 1988 Transient compressible flow in porous materials. Sandia National Laboratories, SAND-83-1788◦UC-45.

Son, S. F., Asay, B. W., Bdzil J. B. & Kober, E. M. 1995 Reaction rate modeling in the deflagration-to-detonation transition in granular energetic materials. In *Decomposition, Combustion, and Detonation Chemistry of Energetic Materials Symposium*, Vol. 418, pp. 313–324. Boston, MA, Materials Research Society.

Sulimov, A. A., Ermolaev, B. S., Borisov, A. A., Korotkov, A. I., Khasainov, B. A. & Khrapovsky, V. E. 1976 On the mechanism of deflagration to detonation transition in gas-permeable high explosive. In *Sixth Symposium (International) on Detonation*. Naval Surface Weapon Center, White Oak, MD, Office of Naval Research, Department of the Navy.

Taylor, J. W. 1962a The burning of secondary explosive powders by a convective mechanism. *Transactions of the Faraday Society* **58,** 561–568.

Taylor, J. W. 1962b A melting stage in the burning of solid secondary explosives. *Combustion and Flame* **6,** 103–107.

Thompson, P. A. 1972 *Compressible-fluid Dynamics*. McGraw-Hill, New York.

Whitham, G. B. 1974 *Linear and Nonlinear Waves*. Wiley, New York.

APPENDIX

Slow-flow Approximation Under Adiabatic Conditions

Again, we are interested in the time and distance scales that are large compared to the permeation scales t_p and x_p. Introducing slow variables

$$s \equiv \epsilon^a \tau, \quad y \equiv \epsilon^b \xi \tag{A1}$$

and scaled dependent variables

$$P = \epsilon^d P_d, \quad R = \epsilon^f R_f, \quad U = \epsilon V, \tag{A2}$$

[10]–[12] with the nozzling term dropped (applied to a bed of constant porosity), become

$$\epsilon^{a+f} \frac{\partial R_f}{\partial s} + \epsilon^{1+b+f} \frac{\partial}{\partial y} (R_f V) = 0, \tag{A3}$$

$$\epsilon^{1+f} R_f \left(\epsilon^a \frac{\partial V}{\partial s} + \epsilon^{1+b} V \frac{\partial V}{\partial y} \right) + \epsilon^{b+d} \frac{1}{\gamma} \frac{\partial P_d}{\partial y} = -\epsilon V, \tag{A4}$$

and

$$\frac{\epsilon^d}{\gamma}\left(\epsilon^a\frac{\partial P_d}{\partial s}+\epsilon^{1+b}V\frac{\partial P_d}{\partial y}\right)-\epsilon^d\left(\frac{P}{R}\right)\left(\epsilon^a\frac{\partial R_f}{\partial s}+\epsilon^{1+b}V\frac{\partial R_f}{\partial y}\right)=\epsilon^2(\gamma-1)V^2 \qquad [A5]$$

where $\epsilon \ll 1$ is not related to the ϵ used earlier, but rather is used here to measure the slowness of the flow. Retaining the full mass conservation equation [A3], yields

$$a = 1 + b. \qquad [A6]$$

Using the fact that empirical correlations on drag finds that in the momentum equation (negligible inertial terms)

$$b + d = 1, \qquad [A7]$$

from which it follows that

$$d + a = 2. \qquad [A8]$$

Since, $1 + a + f > 1$, it therefore follows that the least restrictive long-time scalings has

$$d = 0, \quad b = 1, \quad a = 2, \quad f = 0, \qquad [A9]$$

which then obtains

$$s \equiv \epsilon^2\tau, \quad y \equiv \epsilon\xi,$$
$$P = O(1), \quad R = O(1), \quad U = \epsilon V, \qquad [A10]$$

and yields the flow equations

$$\frac{\partial R}{\partial s}+\frac{\partial}{\partial y}(RV)=0, \qquad [A11]$$

$$\frac{1}{\gamma}\frac{\partial P}{\partial y}=-V, \qquad [A12]$$

and

$$\frac{1}{\gamma}\left(\frac{\partial P}{\partial s}+V\frac{\partial P}{\partial y}\right)-\left(\frac{P}{R}\right)\left(\frac{\partial R}{\partial s}+V\frac{\partial R}{\partial y}\right)=(\gamma-1)V^2. \qquad [A13]$$

Importantly, the inertial terms in the momentum equation did not survive this limit, but all other terms suffer no approximation. Entropy production due to the drag remains in force; the flow is neither isothermal nor isentropic. Eliminating R and V from [A11]–[A13], yields the surprisingly simple result

$$\frac{\partial P}{\partial s}-\frac{\partial}{\partial y}\left(P\frac{\partial P}{\partial y}\right)=0. \qquad [A14]$$

This is a rationally derived low-speed flow result that only assumes adiabatic conditions. It shows that dissipation due to the drag interaction *can not* be neglected based on the slow-flow approximation, as done in previous work.